Thermochemical and Kinetic Analysis of the Acetyl Radical ($CH_3C^{\bullet}O$) + O_2 Reaction System

Jongwoo Lee, Chiung-Ju Chen, and Joseph W. Bozzelli*

Department of Chemical Engineering, Chemistry, and Environmental Science, New Jersey Institute of Technology, Newark, New Jersey 07102

Received: December 7, 2001; In Final Form: April 8, 2002

Thermochemical properties for reactants, intermediates, products, and transition states important in the acetyl radical ($CH_3C^{\bullet}(=O)$) + O_2 reaction system are analyzed with density functional and ab initio calculations, to evaluate reaction paths and kinetics in both oxidation and pyrolysis. Enthalpies of formation ($\Delta H^{\circ}_{f,298}$) are determined using isodesmic reaction analysis at the CBSQ composite and density functional levels. Entropies (S°_{298}) and heat capacities ($C^{\circ}_p(T)$) are determined using geometric parameters and vibrational frequencies obtained at the HF/6-31G(d′) level of theory. Internal rotor contributions are included in S and $C_p(T)$ values. The acetyl radical adds to O_2 to form a $CH_3C(=O)OO^{\bullet}$ peroxy radical with a 35 kcal/mol well depth. The peroxy radical can undergo dissociation back to reactants, decompose to products, $CH_2C=O + HO_2$ via concerted HO_2 elimination (E_a = 34.58 kcal/mol), or isomerize via hydrogen shift (E_a = 26.42) to form a $C^{\bullet}H_2C(=O)OOH$ isomer. This $C^{\bullet}H_2C(=O)OOH$ isomer can undergo β scission to products, $CH_2C=O + HO_2$ (E_a = 31.41), decompose to a cyclic ketone, $\overline{YCOC(=O)}$ + OH via OH elimination (E_a = 19.97, Y = cyclic), decompose to a diradical, $C^{\bullet}H_2CO(O^{\bullet})$ + OH via simple RO−OH bond cleavage (E_a = 27.57), or isomerize back to the $CH_3C(=O)OO^{\bullet}$ isomer. Rate constants are estimated as function of pressure and temperature using quantum Rice−Ramsperger−Kassel analysis for $k(E)$ and master equation for falloff. Important reaction products are stabilization of $CH_3C(=O)OO^{\bullet}$ peroxy adduct at low temperature and, at higher temperatures, formation of a diradical, $C^{\bullet}H_2CO(O^{\bullet})$, + OH and $CH_2C=O + HO_2$ are dominant. $\Delta H^{\circ}_{f,298}$ values are estimated for the following compounds at the CBSQ level: (kcal/mol) $CH_3C^{\bullet}(=O)$ (−3.08), $C^{\bullet}H_2CHO$ (3.52), $CH_3C(=O)OOH$ (-84.80), $CH_3C(=O)OO^{\bullet}$ (−38.57), $C^{\bullet}H_2C(=O)OOH$ (−32.95), and $\overline{YCOC(=O)}$ (-44.42). A mechanism for pyrolysis and oxidation of the acetyl radical is constructed. Reaction of acetyl with O_2 versus unimolecular decomposition is evaluated versus temperature and pressure. Related oxygen bonds in acetyl hydroperoxide are predicted to be stronger than corresponding bonds in alkyl hydroperoxide.

1. Introduction

Important initial products from pyrolysis, oxidation, or photochemical reactions of saturated and unsaturated hydrocarbons are the corresponding radicals. The subsequent reactions of the hydrocarbon radicals with molecular oxygen are complex and often difficult to study experimentally. These reactions often represent the principal pathways of the radical conversion in hydrocarbon combustion[1,2] and atmosphere oxidation.

CH_3CHO is of particular interest in atmospheric chemistry because it is formed as a product of the reaction of O_3 and/or OH with naturally occurring, nonmethane hydrocarbons, especially higher olefins such as isoprene and terpenes.[3,4] The photooxidation of hydrocarbons in photochemical smog also produces acetaldehyde as a major intermediate product. Acetaldehyde is, in addition, a significant product of incomplete combustion processes in diesel engines, aircraft exhausts, power plants, waste combustion, and many other oxidation processes. Acetaldehyde is also one of the important oxidation products of ethane and ethylene. Acetaldehyde and acetyl radicals are important intermediates in the overall breakdown processes of higher molecular weight and C_1 hydrocarbons to CH_2O, CO, CO_2, and H_2O. Acetyl radical reaction with oxygen also serves as model reactions for larger aldehydic systems.

Acetylperoxy radicals $CH_3C(=O)OO^{\bullet}$ (often represented as $CH_3CO_3^{\bullet}$ or CH_3CO_3) are formed as a result of $CH_3C^{\bullet}O$ radical reaction with O_2 and subsequent stabilization of the energized adduct. The $CH_3C^{\bullet}O$ radical is produced in the initial oxidation of acetaldehyde, which is often a product in the photochemical oxidation and combustion of higher carbonyl compounds (acetone, methylvinyl ketone, methylglyoxal, etc.) These peroxy radicals play an important role in atmospheric photooxidation processes:

$$CH_3C^{\bullet}O + O_2 \rightarrow CH_3C(=O)OO^{\bullet}*$$

$$CH_3C(=O)OO^{\bullet}* + M \rightarrow CH_3C(=O)OO^{\bullet} + M$$

These stabilized peroxy radicals react with NO_x when it is present in the atmosphere and in the clean troposphere with other peroxy radicals. Acetylperoxy radicals are the precursor of peroxyacetylnitrite (PAN) an important constituent of pho-

* To whom correspondence should be addressed. E-mail: Bozzelli@njit.edu. Phone: (973)-596-3459. Fax: (973)-642-7170.

10.1021/jp014443g CCC: $22.00
Published on Web 07/13/2002

SCHEME 1: Potential Energy Diagram of Ethyl Radical + O_2 (CBS-Q//B3LYP/6-31G(d,p))

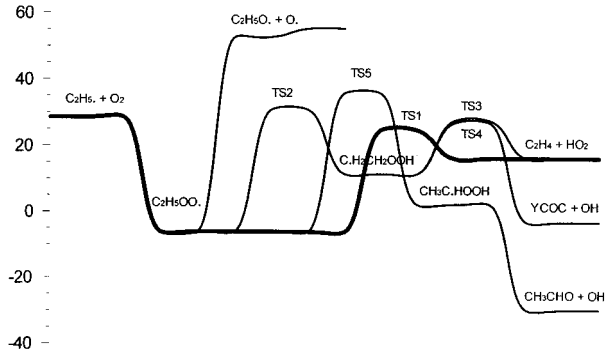

tochemical smog and an air pollutant having important physiological effects. PAN is formed by combination with NO_2[5]:

$$CH_3C(=O)OO^{\bullet} + NO_2 + M \rightarrow CH_3C(=O)OONO_2(PAN) + M$$

Because of its thermal stability at lower temperatures and its photochemical inertness under tropospheric conditions, PAN can act as a temporary reservoir for NO_x and serve as a carrier for transport in colder regions of the troposphere.

Several studies have illustrated that the reactions of ethyl[6−12] and isopropyl[13] radicals at pressures from 1 to 6000 Torr and temperatures from 300 to 900 K exhibit significant negative temperature dependence (NTD) and complex falloff with pressure. We expect acetyl radical reaction with O_2 to have similar complexities.

The ethyl radical + O_2 reaction is the system best characterized in the literature, and it is a useful model with which to compare $CH_3C^{\bullet}O + O_2$ reaction paths and kinetics. Analysis of the $C_2H_5^{\bullet} + O_2$ reaction system[14−16] invokes formation of a chemically activated adduct ($C_2H_5OO^{\bullet}$*), which can be stabilized, dissociate back to $C_2H_5^{\bullet} + O_2$, undergo concerted elimination to $C_2H_4 + HO_2$, or undergo intramolecular hydrogen transfer to hydroperoxide alkyl radical ($C^{\bullet}H_2CH_2OOH$*). The $C^{\bullet}H_2CH_2OOH$* isomer can be stabilized, react to an epoxide YCOC + OH (Y = cyclic), or undergo elimination to ethylene + HO_2. The stabilized adduct ($C_2H_5OO^{\bullet}$) can undergo the same reactions as $C_2H_5OO^{\bullet}$*, but at a lower rate because of its lower energy (Scheme 1).

The hydrogen transfer (to $C^{\bullet}H_2CH_2OOH$) and concerted elimination (to $C_2H_4 + HO_2$) reactions of $C_2H_5OO^{\bullet}$ have tight transition states, relative to the loose transition state of reverse elimination, but the concerted elimination is the only channel that has a barrier which is lower than the entrance channel. At low to moderate temperatures, the $C_2H_5OO^{\bullet}$ will undergo elimination via this low energy path to $C_2H_4 + HO_2$. Reaction of this ethyl peroxy via the H shift channel to a hydroperoxide alkyl radical ($C^{\bullet}H_2CH_2OOH$) has a barrier that is above the entrance channel. All reactions are reversible, and all reverse reactions occur except the epoxide + OH (because of the reactive nature of OH). It is important to note that the $C^{\bullet}H_2$-CH_2OOH isomer can also be formed by addition of HO_2 to ethylene; this $C^{\bullet}H_2CH_2OOH$ can further react with O_2.

The rate of ethyl radical loss decreases significantly with temperature[7] but increases with pressure; this is explained by invoking reversible formation of a weakly bound adduct. The $C_2H_5OO^{\bullet}$* adduct is readily stabilized at low temperatures and atmospheric pressure but dissociates back to reactants at higher temperatures. This rapid dissociation of the peroxy adduct is used in the explanation of the observed negative temperature dependence (NTD) regime in hydrocarbon oxidation. The epoxide (YCOC) is an observed product in this reaction system[17] at least in part formed from the HO_2 addition to ethylene path[18] because in this reaction system, $C_2H_5^{\bullet} + O_2$, $C_2H_4 + HO_2$, as well as adducts $C_2H_5OO^{\bullet}$ and $C^{\bullet}H_2CH_2OOH$ will often exist in a quasiequilibrium under combustion conditions. The Arrhenius *A* factor for direct HO_2 elimination is much lower than that for dissociation of the complex to reactants, but the barrier height is also lower. Stabilization and dissociation back to reactants are dominant paths for the chemically activated adduct, whereas concerted HO_2 elimination is the important reaction channel for the stabilized adduct at lower temperature.

There is very little information on the chemical activation reaction of $CH_3C^{\bullet}O$ radicals with O_2 relative to the ethyl + O_2 system.[19] The oxidation process involves formation of a chemically activated peroxyacetyl radical, $CH_3C(=O)OO^{\bullet}$, which can undergo reactions similar to the ethyl peroxy system. Our analysis shows similarities in well depth for $CH_3C^{\bullet}O$ + O_2 and ethyl radical but significant differences in important reaction paths from that of ethyl + O_2.

2. Previous Studies

$$CH_3C^{\bullet}O + O_2 + M \rightleftharpoons CH_3C(=O)OO^{\bullet} + M \qquad (1)$$

One absolute measurement of k_1 has been reported in the literature; McDade et al.[20] determined $k_1 = (1.2 \pm 0.2) \times 10^{12}$ cm^3/(mol s) in 1−4 Torr He at 298 K. The high-pressure limit value of $k_1 = (3.01 \pm 1.5) \times 10^{12}$ cm^3/(mol s) recommended by the IUPAC panel is based on the absolute measurements of McDade et al.[20] and the pressure dependence of the $C_2H_5^{\bullet}$ + O_2 reaction.[21] The results from two other studies, on the relative reactivity of $CH_3C^{\bullet}O$ with O_2 and Cl_2 [5] and on the rate constant for $CH_3C^{\bullet}O$ with Cl_2,[22] have been combined to give a high-pressure limit rate constant of $k_1 = (1.9 \pm 0.4) \times 10^{12}$ cm^3/(mol s) at room temperature.

Tyndall et al.[23] studied the reaction of the OH radical with methyl glyoxal and acetaldehyde in a low pressure (ca. 3 Torr) flow reactor between 260 and 333 K. They report rate constants for OH abstractions from the parent molecules and also report data on further reactions of the radicals formed from the abstractions. They infer that only the acetyl radical is formed (no indication of formyl methyl radical) and further reaction of acetyl radical with O_2 leads to noticeable regeneration of OH based on observations showing reduced loss of the OH versus time. Chamber experiments by the same group at atmospheric pressure using FTIR detection showed no evidence of OH radical production.[23]

Absolute rate constants of fluorine atom reaction with acetaldehyde were studied by Sehested and co-workers,[24] who report $k_1 = (2.65 \pm 0.4) \times 10^{12}$ cm^3/(mol s) at 295 K and 1000 mbar total pressure of SF_6 using pulse radiolysis combined with transient ultraviolet absorption. They report production of two radicals: formyl methyl at 35% and acetyl at 65% (both ±9%).

Reactions where a chlorine atom is abstracting a hydrogen atom usually have similar *A* factors to that of fluorine and low E_a's, when the reactions are exothermic, as they are in this study. In the case of acetaldehyde, for example, k_{298} for Cl atom abstraction is reported as 4.58×10^{13} [25] at 298 K, whereas abstraction by the F atom is 5.00×10^{13}.[26] The H···Cl bond is 103 kcal/mol, whereas the carbonyl C···H and methyl C···H bonds on acetaldehyde are 88.7 and 95.3 kcal/mol, respectively. Although one might expect some abstraction of the methyl hydrogens by chlorine considering statistical factors, the discus-

sion below suggests this is small and maybe insignificant at atmospheric temperature.

Michael et al.[27] studied the reaction of OH with acetaldehyde in a low-pressure discharge flow reactor using resonance fluorescence to monitor OH. They also studied the further reaction of product radical(s) (generated via the OH reaction) with O_2. The total reaction rate constant for OH with acetaldehyde was $A = 3.3 \times 10^{12}$, with a small negative energy of activation of 610 cal/mol. Michael et al. also report near complete regeneration of the OH radical in the OH + acetaldehyde experiments when O_2 was initially present to further react with the product radical. This OH regeneration was also observed in studies where the Cl atom was used to generate the acetyl radical from acetaldehyde. They considered and rejected possible formation of formyl methyl radicals based on work of Gutman's research group.[28] Slagle and Gutman[28] studied formation of the acetyl radical from acetaldehyde in the reaction of Cl atoms and monitored the radical profiles with photoionization mass spectrometry. Verification of the $CH_3C^{\bullet}O$ radical versus formyl methyl was by use of deuterated acetaldehyde, CD_3CHO. They observed $CD_3C^{\bullet}O$ and could not detect $C^{\bullet}D_2CHO$; although they did not report lower limits of detection, they did indicate $CD_3C^{\bullet}O$ was readily detected.

Alvarez-Idaboy et al.[29] have recently characterized the abstraction reaction of OH + acetaldehyde at the CCSD(T)/6-311++G(d,p)//MP2(FC)/6-311++G(d,p) level of theory. The reaction rate constant was calculated as $k = 8.72 \times 10^{12}$ with a small negative energy of activation, 1.71 kcal/mol. They used the canonical transition state theory as applied to a mechanism involving the formation of a prereactive complex to reproduce the reported experimental results. They indicated that the reaction predominantly occurs by hydrogen abstraction from the carbonyl site, and that OH addition to the carbonyl carbon is unfavorable. The energetics of abstraction of H's on acetaldehyde by OH was also studied by Aloisio and Francisco[30] at the B3LYP//6-311++G(3df,3pd) level of theory. Binding energy (D_o) for $CH_3CHO-HO$ prereactive complex was calculated as 4.0 kcal/mol.

Although the abstraction can occur at two sites, both studies[29,30] report that the dominant reaction is the abstraction from the carbonyl site. They reported that the position of the OH hydrogen atom in the prereactive complex is very far from the methyl hydrogen. In addition, the energy of the methyl C−H bond is about 5 kcal/mol larger than that of the carbonyl C−H bond. (This difference is 6.6 kcal/mol at the CBSQ level of theory in this study.)

Formyl methyl, the other radical that may be formed by abstraction of H atoms from acetaldehyde, was generated by photodissociations of methyl vinyl ether by Zhu and Johnston.[31] $CH_3-O-C_2H_3 + h\nu \Rightarrow CH_3 + C_2H_3O$. Here the vinoxy radical undergoes rapid electron rearrangement to the lower energy form (ca 18 kcal/mol lower): the formyl methyl radical. Kinetic studies on this formyl methyl radical with O_2 show slower reaction, $k' = 1.2 \times 10^{11}$ cm^3/(mol s), relative to the acetyl radical $k_1 = 1 \times 10^{12}$ cm^3/(mol s). This suggests that formyl methyl radicals produced in reactions of Cl atoms, or OH with acetaldehyde will react about one tenth as fast with O_2, probably leading to small or no required correction to kinetic data of the faster acetyl + O_2 reactions. It could also be that the well depth for formyl methyl + O_2 is very shallow and the reverse reaction is fast, thus leading to low observed adduct yields.

This study focuses on the reaction mechanism of the acetyl radical association with O_2. Thermochemical properties are estimated for reactants, intermediates, products, and transition states in the reaction paths using ab initio and density functional calculations. The thermochemical parameters are used to calculate high-pressure limit rate constants using canonical transition state theory (TST). Rate constants as a function of temperature and pressure are estimated using a multifrequency quantum RRK analysis for k(E) and master equation analysis for falloff. The data at relevant pressures and temperatures should be useful to both atmospheric and combustion models.

3. Calculation Methods

Enthalpies of formation ($\Delta H^{\circ}_{f,298}$) for reactants, intermediate radicals, transition states, and products are calculated using the CBS-Q composite method and density functionals. The initial structure of each compound or transition state is determined using ROHF or UHF/PM3 in MOPAC,[32] followed by optimization and vibrational frequency calculation at the HF/6-31G(d′) level of theory using Gaussian 94.[33] The prime in 6-31G(d′) indicates the basis set orbitals of Petersson et al.[34−35] Transition state geometries are identified by the existence of only one imaginary frequency, structure information, and the TST reaction coordinate vibration information. Zero-point vibrational energies (ZPVE) are scaled by 0.91844 as recommended by Petersson et al.[36] Single-point energy calculations are carried out at the B3LYP/6-31G(d). The complete basis set (CBS-Q) method of Petersson and co-workers for computing accurate energies[37,38] is chosen as the determining enthalpies used in our kinetic analysis.

The CBS-Q calculation sequence is performed on a geometry determined at the MP2/6-31G(d′) level followed by single-point calculations at the theory level of QCISD(T)/6-31+G(d′), MP4-(SDQ)/CBSB4, and MP2/CBSB3 CBSExtrap = (Nmin=10,-Pop) including corrections for unpaired electron and spin contamination in intermediate overlap (i.e., $0 < {}^{\alpha\beta}S_{ij} < 1$) between the α and β spin orbitals.[39]

3.1. Determination of the Enthalpy of Formation. Isodesmic reactions are used to determine the enthalpy of formation ($\Delta H^{\circ}_{f,298}$) for parent and radical species. $\Delta H^{\circ}_{f,298}$ for estimation of $CH_3C(=O)OOH$ is by

$$CH_3C(=O)OOH + CH_3CH_2OH \leftrightarrow CH_3C(=O)OH + CH_3CH_2OOH \quad (2)$$

$\Delta H^{\circ}_{f,298}$ for estimation of $C^{\bullet}H_2C(=O)OOH$ [$^{\bullet}$: radical site] is by

$$C^{\bullet}H_2C(=O)OOH + CH_3CH_3 \leftrightarrow CH_3C(=O)OOH + CH_3C^{\bullet}H_2 \quad (3)$$

$\Delta H^{\circ}_{f,298}$ for estimation of $CH_3C(=O)OO^{\bullet}$ is by

$$CH_3C(=O)OO^{\bullet} + CH_3OOH \leftrightarrow CH_3C(=O)OOH + CH_3OO^{\bullet} \quad (4)$$

The working reactions for estimation of $\Delta H^{\circ}_{f,298}$ on $CH_3C^{\bullet}O$ are

$$CH_3C^{\bullet}O + CH_3CH_3 \leftrightarrow CH_3CHO + CH_3C^{\bullet}H_2 \quad (5)$$

$$CH_3C^{\bullet}O + CH_3OH \leftrightarrow CH_3CHO + C^{\bullet}H_2OH \quad (6)$$

$$CH_3C^{\bullet}O + CH_3C(=O)CH_3 \leftrightarrow CH_3CHO + C^{\bullet}H_2C(=O)CH_3 \quad (7)$$

TABLE 1: Activation Energies and Enthalpies of Transition States in CBSQ Calculation (Units in kcal/mol)

reactant	transition state (TS)	product	E_a	$\Delta H^\circ_{f,298}$ of TS
$CH_3C(=O)OO^\bullet$	$TCC(=O)OO^\bullet$	$C^\bullet H_2C(=O)OOH$	26.42	−12.15
$CH_3C(=O)OO^\bullet$	TCCO−OOH[a]		34.58	−3.99
$C^\bullet H_2C(=O)OOH$	TYCOC(=O)−OH[a]		19.97	−12.98
$C^\bullet H_2C(=O)OOH$	$TC^\bullet CO-OOH$[a]		31.41	−1.54

[a] The activation energy and enthalpy for this transition state is estimated by taking the difference of total energy with ZPVE and thermal correction between the transition state and reactant (peroxy/hydroperoxide isomer).

SCHEME 2: $\Delta H^\circ_{f,TS}$ (TCC(=O)OO•) Calculation

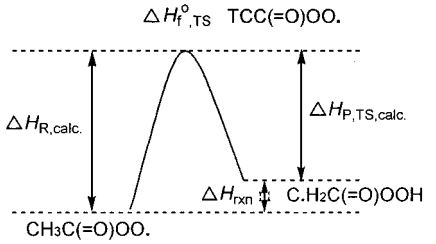

$$\Delta H_{R',TS,calc.} = \Delta H_{rxn}\ (\text{Reactant -> TS}) + \Delta H_{rxn}$$

$$\Delta H_{P,TS,calc.} = \Delta H_{rxn}\ (\text{Product -> TS})$$

$$\Delta H_f^\circ{}_{TS} = (\Delta H_{R',TS,calc.} + \Delta H_{P,TS,calc.})\ /\ 2$$

The working reactions for estimation of $\Delta H^\circ_{f,298}$ on $C^\bullet H_2CHO$ are

$$C^\bullet H_2CHO + CH_3CH_3 \leftrightarrow CH_3CHO + CH_3C^\bullet H_2 \quad (8)$$

$$C^\bullet H_2CHO + CH_3OH \leftrightarrow CH_3CHO + C^\bullet H_2OH \quad (9)$$

$$C^\bullet H_2CHO + CH_3C(=O)CH_3 \leftrightarrow CH_3CHO + C^\bullet H_2C(=O)CH_3 \quad (10)$$

The method of isodesmic reactions relies upon the similarity of the bonding environments in the reactants and products that leads to cancellation of systematic errors from the ab initio MO calculations.[40] It also results in a higher accuracy in estimates of $\Delta H^\circ_{f,298}$ than heats of atomization. The basic requirement of the isodesmic reaction is that the number of bonds of each formal chemical bond type is conserved in the reaction. In reaction 2, ab initio calculations with ZPVE and thermal correction are performed on all four compounds in the reaction. $\Delta H^\circ_{f,298}$ of three of the compounds in reaction 2, excepting the target molecule, $CH_3C(=O)OOH$ in (2), have been experimentally or theoretically determined. The unknown $\Delta H^\circ_{f,298}$ of $CH_3C(=O)OOH$ is obtained with the calculated $\Delta H^\circ_{rxn(298)}$ and known $\Delta H^\circ_{f,298}$ of the three reference compounds. The $C^\bullet H_2C(=O)OOH$, $CH_3C(=O)OO^\bullet$, $CH_3C^\bullet O$, and $C^\bullet H_2CHO$ radicals are calculated in the same manner.

Enthalpies of Transition States. $\Delta H^\circ_{f,298}$'s of transition state structures are estimated by evaluation of $\Delta H^\circ_{f,298}$ of the stable radical adducts from the working reaction analysis above, plus the difference of total energies with ZPVE and thermal correction between these radical species and the transition state. The method is illustrated for the H-shift transition state $TCC(=O)OO^\bullet$ in Scheme 2.

Calculation of the enthalpy of formation for $TCC(=O)OO^\bullet$ is not taken as the calculated energy difference between reactant and transition state. The absolute enthalpies of reactant and product are first estimated using isodesmic reaction analysis [(3) and (4)]. ΔH_{rxn} is taken from ΔH_f° values determined from the separate isodesmic reactions. $\Delta H_{R',TS,calc.}$ is the difference between the calculated energy of the transition state and reactant plus ΔH_{rxn} ($\Delta H^\circ_{f,product} - \Delta H^\circ_{f,reactant}$). $\Delta H_{P,TS,calc.}$ is the difference between the calculated energy of the transition state and product. $\Delta H^\circ_{f,TS}$ is calculated by an average of two values $\Delta H_{R',TS,calc.}$ and $\Delta H_{P,TS,calc}$. (Table 1)

3.2. Determination of Entropy and Heat Capacity. The contributions of external rotation and vibrations to entropies and heat capacities are calculated from scaled vibration frequencies and moments of inertia for the optimized HF/6-31G(d′) structures. Contributions from frequencies corresponding to hindered internal rotation are replaced with values calculated from the method of Pitzer and Gwinn[41] for S and $C_p(T)$. The number of optical isomers and spin degeneracy of unpaired electrons are also incorporated.

3.3. High-Pressure Limit *A* Factor (A_∞) and Rate Constant (k_∞) Determination. For the reactions where thermochemical properties of the transition state are calculated by ab initio or density functional methods, k_∞'s are fit by three parameters A_∞, n, and E_a over temperature range from 298 to 2000K, $k_\infty = A_\infty(T)^n \exp(-E_a/RT)$. Entropy differences between reactant and transition state are used to determine the preexponential factor, A, via canonical transition state theory (TST)

$$A = (k_bT/h_p)\exp(\Delta S^\ddagger/R), \quad E_a = \Delta H^\ddagger$$

(h_p is the Planck constant and k_b is the Boltzmann constant.) Treatment of the internal rotors for S and $C_p(T)$ is important here because these internal rotors are often lost in the cyclic transition state structures.

3.4. Kinetic Analysis. The potential energy surface and thermochemical properties are evaluated, and forward or reverse rate constants (high-pressure limit) for each elementary reaction step are determined. Multifrequency quantum Rice−Ramsperger−Kassel (QRRK) analysis for $k(E)$ with master equation analysis[42] for falloff with a 0.5 kcal energy grain is used to obtain rate constants as a function of temperature and pressure, for the separate chemical activation and dissociation reactions.

The QRRK analysis is described by Chang et al.[43] It is shown to yield reasonable results and provides a framework by which the effects of temperature and pressure can be evaluated in complex reaction systems. The QRRK code utilizes a reduced set of three vibration frequencies which accurately reproduce the molecules'(adduct) heat capacity and include one external rotation in calculation of density of states $\rho(E)/Q$. Comparisons of ratios of these $\rho(E)/Q$ (partition function Q) with direct count $\rho(E)/Q$ are shown to be in good agreement.[44] Nonlinear Arrhenius effects resulting from changes in the thermochemical properties of the respective transition state relative to the adduct with temperature are incorporated using a two parameter Arrhenius preexponential factor (A, n) in AT^n.

Tunneling is applied for the intramolecular hydrogen atom transfer reactions of $TCC(=O)OO^\bullet$ and $TC^\bullet CHOS$ and hydrogen atom dissociation reactions, $TC^\bullet CHO-H$ and $TCC^\bullet O-H$. Tunneling effects are taken into account using the Erwin−Henry code[45] to determine high-pressure limit rate constant (k_∞). This program is based on Eckart's one-dimensional potential function.[46] Eckart evaluated in closed form an expression for the

probability $k(E)$ of crossing the barrier for a particle of energy E. The Erwin−Henry code requires input of vibrational frequencies, moments of inertia, and total energies at 0 K of reactants, transition states, and products; imaginary frequencies are also required. Total energies are obtained from the CBSQ composite method, and vibrational frequencies and moments of inertia are obtained from HF/6-31G(d′) level of calculation. Schwartz et al. note that calculated vibrational frequencies corresponding to the reaction coordinate at the HF/6-31G(d) level of theory need to be reduced by $^1/_2$−$^1/_3$ for calculated rate constant to match experimental data in abstraction reactions.[47]

4. Results and Discussion

4.1. Geometries of Intermediate Radicals and Transition States. Figures 1S and 2S (Supporting Information) show the MP2/6-31G(d′) optimized geometries of the two intermediate radicals, $CH_3C(=O)OO^{\bullet}$ and $C^{\bullet}H_2C(=O)OOH$, respectively.

All bond lengths are from MP2/6-31G(d′) determined geometries except TYCOC(=O)-OH.

Transition states are identified as follows:

TCC(=O)OO•: peroxy radical $CH_3C(=O)OO^{\bullet}$ isomerizes to form a $C^{\bullet}H_2C(=O)OOH$ isomer via hydrogen shift.

TCCO−OOH: peroxy radical $CH_3C(=O)OO^{\bullet}$ decomposes to products, $CH_2CO + HO_2$ via concerted HO_2 elimination.

TC•CO−OOH: $C^{\bullet}H_2C(=O)OOH$ isomer undergoes β scission to products, $CH_2CO + HO_2$

TYCOC(=O)−OH: $C^{\bullet}H_2C(=O)OOH$ isomer reacts to products, $YCOC(=O) + OH$ via intramolecular addition and OH elimination.

TC•CHOS: formyl methyl radical $C^{\bullet}H_2CHO$ isomerizes to form a $CH_3C^{\bullet}O$ isomer via hydrogen shift.

TC•CHO−H: $C^{\bullet}H_2CHO$ undergoes β scission to products, $CH_2CO + H$

TCC•O−H: $CH_3C^{\bullet}O$ isomer undergoes β scission to products, $CH_2CO + H$

TCH_3−CO: $CH_3C^{\bullet}O$ isomer decomposes to products, $CH_3 + CO$

Figure 3S shows the transition state (TS) structure for the H shift isomerization reaction, $TCC(=O)OO^{\bullet}$. The H_6 atom is in a bridge structure shifting from C_1 to the radical site on O_5. The leaving bond length H_6-C_1 is calculated as 1.27 Å where the H−C bond length in $CH_3C(=O)OO^{\bullet}$ is 1.09 Å. The forming bond H_6-O_5 is calculated as 1.25 Å,where the H−O bond in the stable $C^{\bullet}H_2C(=O)OOH$ is 0.97 Å.

Figure 4S shows the TS structure for direct HO_2 elimination from the peroxy adduct: $CH_3C(=O)OO^{\bullet} \rightarrow CH_2CO + HO_2$, TCCO−OOH. The C_1-H_8 bond is calculated as 1.43 Å, where the C−H bond length in $CH_3C(=O)OO^{\bullet}$ is 1.09 Å. The transition state C_2-O_6 bond is 2.32 Å, and the O_6-O_7 bond is 1.28 Å.

Figure 5S shows the B3LYP/6-31G(d) determined geometry of the TS for formation of the epoxide carbonyl; the alkyl carbon radical attacks peroxy oxygen bonded to carbon to form a three-membered ring and OH elimination $C^{\bullet}H_2C(=O)OOH \rightarrow YCOC(=O) + OH$, TYCOC(=O)−OH. The transition state O_4-O_7 bond length is calculated as 1.84 Å, and the O−O bond length in $C^{\bullet}H_2C(=O)OOH$ is calculated as 1.46 Å. The forming C_3-O_4 bond is calculated as 1.95 Å, and the C−O bond length in YCOC(=O) is calculated as 1.54 Å.

Figure 6S shows the TS structure for β scission to products, $CH_3C^{\bullet}O \rightarrow CH_2CO + H$, TCC•O−H. The transition state C_1-C_4 bond length is calculated as 1.34 Å, and the C−C bond lengths in CH_2CO and $CH_3C^{\bullet}O$ are calculated as 1.31 and 1.52 Å. The leaving C_1-H_5 bond is calculated as 1.70 Å.

TABLE 2: Enthalpies of Formation for the Reference Moleculesin the Isodesmic Reactions

compounds	$\Delta H^{\circ}_{f,298}$ (kcal/mol)
CH_3CH_2OH	-56.17 ± 0.10[48] [a]
$CH_3C(=O)OH$	-103.56 ± 0.32[b]
CH_3CH_3	-20.24 ± 0.10[51] [a]
CH_3CHO	-39.72 ± 0.12[48] [a]
$C^{\bullet}H_2OH$	-3.97 ± 0.22[53]
$C^{\bullet}H_2C(=O)CH_3$	-8.53 ± 1.15[54]
CH_3CH_2OOH	-39.70 ± 0.16[18]
$CH_3C^{\bullet}H_2$	28.80 ± 0.50[52]
CH_3OH	-48.16 ± 0.07[49]
$CH_3C(=O)CH_3$	-51.94 ± 0.17[49]

[a] The uncertainties are evaluated from ref 49. [b] Average of −103.32,[48] −103.44,[49] and −103.92[50].

Figure 7S shows the TS structure for β scission to products, $C^{\bullet}H_2CHO \rightarrow CH_2CO + H$, TC•CHO−H. The transition state C_1-C_4 bond length is calculated as 1.35 Å, and the C−C bond lengths in CH_2CO and $C^{\bullet}H_2CHO$ are calculated as 1.31 and 1.47 Å. The leaving C_4-H_5 bond is calculated as 1.64 Å.

Figure 8S shows the TS structure for the H shift isomerization reaction, TC•CHOS. The H_4 atom is in a bridge structure shifting from C_2 to the radical site on C_1. The leaving H_4-C_2 bond is calculated as 1.27 Å. The forming H_4-C_1 bond is calculated as 1.50 Å.

Figure 9S shows the TS structure for decomposing to products, $CH_3C^{\bullet}O \rightarrow CH_3 + CO$, TCH_3−CO. The leaving C_1-C_2 bond is calculated as 2.11 Å.

4.2. Enthalpy of Formation ($\Delta H^{\circ}_{f,298}$) using Calculated Total Energies and Isodesmic Reactions. The total energies at 0 K including scaled ZPVEs, thermal corrections to 298.15 K, and total energies at 298 K are shown in Table IS (Supporting Information) for CBSQ calculations. Frequencies are scaled by 0.91844 for HF/6-31G(d′) determined frequencies as recommended by Petersson et al.[36]

The evaluated enthalpies of formation for the reference molecules and radicals in the isodesmic reactions are listed in Table 2. The evaluated reaction enthalpies and enthalpies of formation in the isodesmic reactions are listed in Table 3.

A low or zero $\Delta H^{\circ}_{rxn,298}$ in the working reactions suggests good cancellation of errors in the reaction analysis leading to accurate $\Delta H^{\circ}_{f,298}$ values, and supports the hypothesis of group additivity. As an example, $\Delta H^{\circ}_{f,298}$ $[CH_3C(=O)OOH]$ is evaluated from

$$\Delta H^{\circ}_{f,rxn,298} = \Delta H^{\circ}_{f,298}[CH_3C(=O)OH] + \Delta H^{\circ}_{f,298}[CH_3CH_2OOH] - \Delta H^{\circ}_{f,298}[CH_3C(=O)OOH] - \Delta H^{\circ}_{f,298}[CH_3CH_2OH]$$

$$\Delta H^{\circ}_{f,rxn,298} = -2.29(\text{CBSQ}) \text{ and } -3.88(\text{B3LYP})$$

$$\Delta H^{\circ}_{f,rxn,298} = -103.56 + (-39.70) - X - (-56.17) \text{ kcal/mol} \quad (11)$$

The enthalpies of formation of $CH_3C(=O)OOH$ obtained are −84.80 and −83.21 kcal/mol by CBSQ and B3LYP/6-31G(d), respectively.

Enthalpies of formation of the two intermediate radicals, $C^{\bullet}H_2C(=O)OOH$ and $CH_3C(=O)OO^{\bullet}$ by CBSQ and B3LYP/6-31G(d), are obtained from the use of isodesmic reactions 3 and 4 and values of reference species in Table 2. The bond dissociation energies of reference species in these reactions are as follows: C_2H_5-H and CH_3OO-H are 101.1 and 86.6 kcal/

TABLE 3: Reaction Enthalpies and Enthalpies of Formation in the Isodesmic Reactions (Units in kcal/mol)

working reaction series	$\Delta H^\circ_{rxn,298}$ B3LYP	$\Delta H^\circ_{rxn,298}$ CBSQ	$\Delta H^\circ_{f,298}$ B3LYP	$\Delta H^\circ_{f,298}$ CBSQ
$CH_3C(=O)OOH$ + $CH_3CH_2OH \leftrightarrow CH_3C(=O)OH + CH_3CH_2OOH$	−3.88	−2.29	−83.21	**−84.80**
$C^\bullet H_2C(=O)OOH$ + $CH_3CH_3 \leftrightarrow CH_3C(=O)OOH + CH_3C^\bullet H_2$	−1.54	−2.85	−32.67	**−32.95**
$CH_3C(=O)OO^\bullet$ + $CH_3OOH \leftrightarrow CH_3C(=O)OOH + CH_3OO^\bullet$	−11.19	−11.73	−37.52	**−38.57**
$CH_3C^\bullet O$ + $CH_3CH3 \leftrightarrow CH_3CHO + CH_3C^\bullet H2$		12.26		−2.94
$CH_3C^\bullet O$ + $CH_3OH \leftrightarrow CH_3CHO + C^\bullet H_2OH$		7.25		−2.78
$CH_3C^\bullet O$ + $CH_3C(=O)CH3 \leftrightarrow CH_3CHO + C^\bullet H_2C(=O)CH_3$		7.20		−3.51
average for $CH_3C^\bullet O$				**−3.08 ± 0.38**
$C^\bullet H_2CHO$ + $CH_3CH_3 \leftrightarrow CH_3CHO + CH_3C^\bullet H_2$		5.66		3.66
$C^\bullet H_2CHO$ + $CH_3OH \leftrightarrow CH_3CHO + C^\bullet H_2OH$		0.65		3.82
$C^\bullet H_2CHO$ + $CH_3C(=O)CH3 \leftrightarrow CH_3CHO + C^\bullet H_2C(=O)CH_3$		0.60		3.09
average for $C^\bullet H_2CHO$				**3.52 ± 0.38**

TABLE 4: Ideal Gas Phase Thermodynamic Properties Obtained by CBSQ Calculation and by Therm[a]

species (s, e, OI)[g]		$\Delta H^\circ_{f,298}$ [b]	S°_{298} [c]	C_{p300} [c]	C_{p400}	C_{p500}	C_{p600}	C_{p800}	C_{p1000}	C_{p1500}
CH_3CHO	TVR[d]		57.97[g]	11.58	14.29	16.88	19.20	22.98	25.80	30.10
(3,0,1)	internal rotor 1[f]		5.16	1.44	1.30	1.23	1.17	1.10	1.07	1.03
	total	−39.72	63.13	13.02	15.59	18.11	20.37	24.08	26.87	31.13
	THERM	−39.18	63.13	13.22	15.71	18.22	20.47	24.22	26.97	
$CH_3C^\bullet O$	TVR		58.82	11.12	13.24	15.24	17.01	19.90	22.07	25.39
(3,1/2,1)	internal rotor 1		5.45	1.16	1.10	1.06	1.04	1.02	1.01	1.00
	total	−3.08	64.27	12.28	14.34	16.30	18.05	20.92	23.08	26.39
	THERM	−2.54	64.27	12.28	14.34	16.30	18.05	20.92	23.08	
$C^\bullet H_2CHO$	TVR		61.99	13.10	15.79	18.04	19.86	22.63	24.62	27.66
(1,1/2,1)	total	3.52	61.99	13.10	15.79	18.04	19.86	22.63	24.62	27.66
	THERM	4.06	61.99	13.10	15.79	18.04	19.86	22.63	24.62	
$CH_3C(=O)OOH$	TVR		66.93	15.50	19.22	22.49	25.25	29.52	32.59	37.27
(3,0,2)	internal rotor 1,2,3		9.65	5.53	6.06	6.27	6.30	6.06	5.64	4.70
	total	−84.80	76.58	21.03	25.28	28.76	31.55	35.58	38.23	41.97
	THERM	−84.80	76.58	21.03	25.28	28.76	31.55	35.58	38.23	
$CH_3C(=O)OO^\bullet$	TVR		66.69	15.34	18.84	21.87	24.38	28.18	30.86	34.77
(3,1/2,1)	internal rotor 1,2		8.87	4.14	4.38	4.46	4.43	4.21	3.90	3.22
	total	−38.57	75.56	19.48	23.22	26.33	28.81	32.39	34.76	37.99
	THERM	−38.57	75.56	19.48	23.22	26.33	28.81	32.39	34.76	
$C^\bullet H_2C(=O)OOH$	TVR		70.45	15.79	19.14	21.85	24.01	27.19	29.43	32.85
(1,1/2,2)	internal rotor 1,2,3		8.80	6.00	6.39	6.50	6.46	6.15	5.69	4.72
	total	−32.95	79.25	21.79	25.53	28.35	30.47	33.34	35.12	37.57
	THERM	−32.95	78.02	22.07	25.82	28.60	30.67	33.46	35.17	
CH_2CO	TVR		57.57	12.26	14.10	15.61	16.85	18.81	20.29	22.61
(2,0,1)	total		57.57	12.26	14.10	15.61	16.85	18.81	20.29	22.61
	THERM	−11.80	57.81	12.68	14.77	16.43	17.75	19.65	20.92	22.91
$TCC(=O)OO^\bullet$	TVR		72.28	18.52	22.50	25.75	28.32	32.02	34.46	37.79
(1,1/2,2)	total	−12.15	72.28	18.52	22.50	25.75	28.32	32.02	34.46	37.79
TCCO−OOH	TVR		76.34	20.04	23.37	26.14	28.41	31.83	34.20	37.57
(1,1/2,2)	total	−3.99	76.34	20.04	23.37	26.14	28.41	31.83	34.20	37.57
$TC^\bullet CO-OOH$	TVR		74.11	18.14	20.96	23.20	25.00	27.76	29.80	33.03
(1,1/2,2)	internal rotor 1,2		5.07	3.83	4.19	4.41	4.52	4.47	4.20	3.47
	total	−1.54	79.18	21.97	25.15	27.61	29.52	32.23	34.00	36.50
$CH_3C(=O)O^\bullet$	TVR		62.80	12.71	15.42	17.91	21.10	23.58	26.16	30.15
(3,1/2,1)	internal rotor 1		5.62	1.08	1.05	1.03	1.02	1.01	1.00	1.00
	total	−41.35	68.42	13.79	16.47	18.94	22.12	24.59	27.16	31.15
	THERM	−51.38	63.56	14.78	17.67	20.28	22.42	25.81	28.19	
YCOC(=O)	TVR		62.29	11.95	14.65	17.06	19.06	22.10	24.24	27.42
(1,0,1)	total	−44.42	62.29	11.95	14.65	17.06	19.06	22.10	24.24	27.42
$C^\bullet H_2C(=O)O^\bullet$	TVR		66.14	14.53	17.17	19.34	21.10	23.69	25.50	28.17
(1,1,1)	total	−14.87	66.14	14.53	17.17	19.34	21.10	23.69	25.50	28.17
TYCOC(=O)-OH	TVR		73.08	18.74	21.97	24.50	26.48	29.39	31.47	34.77
(1,1/2,1)	internal rotor 1		4.31	1.46	1.30	1.20	1.14	1.08	1.05	1.02
	total	−12.98	77.39	20.20	23.27	25.70	27.62	30.47	32.52	35.79
$TC^\bullet CHOS$	TVR		61.32	12.12	14.47	16.59	18.40	21.21	23.21	26.11
(1,1/2,1)	total	43.03	61.32	12.12	14.47	16.59	18.40	21.21	23.21	26.11
$TC^\bullet CHO-H$	TVR		64.09	15.29	17.59	19.33	20.71	22.79	24.31	26.64
(1,1/2,1)	total	44.01	64.09	15.29	17.59	19.33	20.71	22.79	24.31	26.64
$TCC^\bullet O-H$	TVR		63.25	14.69	17.05	18.88	20.34	22.53	24.12	26.54
(1,1/2,1)	total	40.09	63.25	14.69	17.05	18.88	20.34	22.53	24.12	26.54
TCH3−CO	TVR		60.70	12.22	13.92	15.42	16.75	18.99	20.78	23.69
(3,1/2,1)	internal rotor 1		5.45	1.16	1.10	1.06	1.04	1.02	1.01	1.00
	total	13.56	66.15	13.38	15.02	16.48	17.79	20.01	21.79	24.69

[a] Thermodynamic properties are referred to a standard state of an ideal gas of pure enantiometer at 1 atm. Therm values for stable species are included for comparison (refs 56 and 57). [b] Units in kcal/mol. [c] Units in cal/mol K. [d] Sum of contributions from translations, vibrations, and external rotations. [f] Contribution from internal rotation. [g] Symmetry number, optical isomer, and electronic spin are taken into account, $-R \ln(s)$, $R \ln 2$, and $R \ln 2$, respectively. s = number of symmetry, e = electronic spin, OI = number of optical isomer.

TABLE 5: Moments of Inertia (amu A^2) and Rotational Barriers (kcal/mol) for Internal Rotors

species	rotor	I_A	I_B	V	n^a
CH_3CHO	CH_3 -C(=O)H	3.12	18.90	1.20	6
$CH_3C^{\bullet}O^b$	CH_3 -C$^{\bullet}$(=O)	3.12	12.63	0.55	3
$CH_3C(=O)OOH^c$	CH_3 -C(=O)OOH	3.12	130.14	3.18	3
	$CH_3C(=O)$- -OOH	44.19	1.56	5.46	1
	$CH_3C(=O)O$- -OH	100.00	0.92	7.15	1
$CH_3C(=O)OO^{\bullet}$	CH_3 -C(=O)OO$^{\bullet}$	3.12	126.74	4.00	3
	$CH_3C(=O)$- -OO$^{\bullet}$	44.19	23.30	7.00	1
$C^{\bullet}H_2C(=O)OOH$	$C^{\bullet}H_2$ -C(=O)OOH	1.75	130.14	3.18	2
	$C^{\bullet}H_2C(=O)$- -OOH	42.44	1.56	5.46	2
	$C^{\bullet}H_2C(=O)O$- -OH	100.00	0.92	7.15	1
TC$^{\bullet}$CO−OOH	$C.H_2C(=O)$- -OOH	42.44	1.56	5.46	2
	$C.H_2C(=O)O$- -OH	100.00	0.92	7.15	1
$CH_3C(=O)O^{\bullet}$	CH_3 -C(=O)O$^{\bullet}$	3.12	38.12	0.48	6
TYCOC(=O)−OH	OH- -YCOC(=O)	0.98	61.8	1	2
TCH_3−CO	CH_3 -C$^{\bullet}$(=O)	3.12	12.63	0.55	3

[a] *n*: foldness. [b] "•" stands for radical site. [c] "=" stands for double bonding(C=O).

mol, respectively.[51,52,55] The data results in enthalpy values of −32.95 and −32.67 for $C^{\bullet}H_2C(=O)OOH$ and −38.57 and −37.52 for $CH_3C(=O)OO^{\bullet}$, by CBSQ and B3LYP/6-31G(d), respectively, with bond energies being surprisingly strong, 103.95 and 98.33, respectively.

We use the working reactions 5−7 and 8−10 to estimate enthalpy of $CH_3C^{\bullet}O$ and $C^{\bullet}H_2CHO$ radical species with the CBSQ composite method.

The average values of $\Delta H^{\circ}_{f,298}$ from three isodesmic reactions for $CH_3C^{\bullet}O$ and $C^{\bullet}H_2CHO$ are −3.08 and 3.52 kcal/mol by CBSQ, respectively (Table 3).

4.3. Entropy ($S^{\circ}_{(298)}$) and Heat Capacity ($C_p(T)$, 300 ≤ T/K ≤ 1500). $S^{\circ}_{(298)}$ and $C_p(T)$'s are calculated based on vibration frequencies and moments of inertia of the optimized HF/6-31G(d′) structures (Tables IIS and IIIS).

The calculation results using MP2/6-31G(d′) determined geometries and HF/6-31G(d′) determined frequencies are summarized in Table 4. TVR represents the sum of the contributions from translation, vibrations and external rotations for $S^{\circ}_{(298)}$ and $C_p(T)$'s. Symmetry, number of optical isomers, and electronic spin are incorporated in the estimation of $S^{\circ}_{(298)}$ as described in Table 4. Torsion frequency vibrations are omitted in these calculations; instead, contributions from internal rotation for $S^{\circ}_{(298)}$ and $C_p(T)$'s are calculated based on rotational barrier heights, moments of inertia of the rotors using the method of Pitzer and Gwinn,[41] data on these parameters are listed in Table 5 with internal rotor contributions noted in Table 4.

4.4. Energy Diagram for $CH_3C^{\bullet}O + O_2$ Reaction System. The overall energy diagram for the $CH_3C^{\bullet}O + O_2$ reaction is illustrated in Figure 1 where enthalpies of formation are from CBSQ calculations and in units of kcal/mol. The acetyl radical $CH_3C^{\bullet}O$ ($\Delta H^{\circ}_{f,298}$ = −3.08 kcal/mol) adds to O_2 to form a $CH_3C(=O)OO^{\bullet}$ peroxy radical with a 35.5 kcal/mol well depth. This peroxy radical can undergo dissociation back to reactants, decompose to products, $CH_2CO + HO_2$ via concerted HO_2 elimination with a barrier, (E_a = 34.58) or isomerize via hydrogen shift (E_a = 26.42) to form a $C^{\bullet}H_2C(=O)OOH$ isomer ($\Delta H^{\circ}_{f,298}$ = −32.95).

The $C^{\bullet}H_2C(=O)OOH$ isomer can undergo β scission to products, $CH_2CO + HO_2$ (E_a = 31.41), decompose to a cyclic ketone, YCOC(=O) + OH via OH elimination (E_a = 19.97, Y = cyclic), decompose to a diradical, $C^{\bullet}H_2CO(O^{\bullet}) + OH$ via simple RO−OH bond cleavage (E_a = 27.57), or isomerize via hydrogen shift (E_a = 20.80), to form a $CH_3C(=O)OO^{\bullet}$ isomer.

4.5. Comparison of $C_2H_5 + O_2$ and $CH_3C^{\bullet}O + O_2$. The $C_2H_5^{\bullet} + O_2$ [58] and $CH_3C^{\bullet}O + O_2$ reaction systems have some similarities and some significant differences. The $C_2H_5^{\bullet} + O_2$ and $CH_3C^{\bullet}O + O_2$ reactions have similar well depths, 35.3 and 35.5 kcal/mol, respectively. The H shift isomerization and concerted HO_2 elimination reaction paths for the $C_2H_5OO^{\bullet}$ and $CH_3C(=O)OO^{\bullet}$ have major differences in the barriers. The hydrogen shift in ethylperoxy, $C_2H_5OO^{\bullet}$, to $C^{\bullet}H_2CH_2OOH$ and the barrier for HO_2 molecular elimination, to $C_2H_4 + HO_2$, are 37.05 and 30.93 kcal/mol, respectively. The HO_2 elimination is clearly a more important first step in the ethyl system. In our acetyl radical system, the H shift from $CH_3C(=O)OO^{\bullet}$ to $C^{\bullet}H_2C(=O)OOH$ and HO_2 molecular elimination to $CH_2CO + HO_2$ have barriers, 26.42 and 34.58 kcal/mol, respectively. The lowering of the H shift barrier is partially due to the lower C−H bond of the methyl in the acetyl system. The hydrogen shift is important in this acetyl radical system.

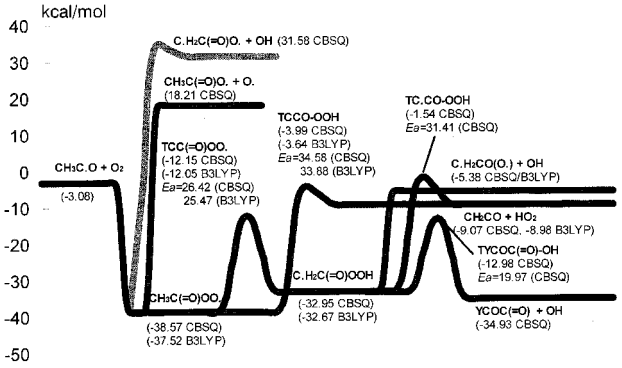

Figure 1. Potential energy diagram $CH_3C^{\bullet}O + O_2$.

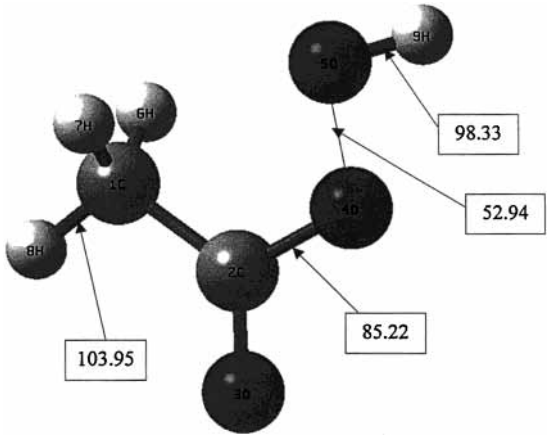

Figure 2. Bond dissociation energy of $CH_3C(=O)OOH$ (units: kcal/mol).

Rienstra-Kiracofe et al.[14] recently studied the $C_2H_5^{\bullet} + O_2$ reaction system with the CCSD and CCSD(T) ab initio methods. They showed that the concerted HO_2 elimination path from $C_2H_5OO^{\bullet}$ is energetically preferred and is also the only mechanism consistent with experimental observations of a negative temperature coefficient.[14] They reported a 30.5 kcal/mol well depth at 0 K; we use vibration frequencies of $C_2H_5^{\bullet}$, O_2, and $C_2H_5OO^{\bullet}$ from the HF/6-31G(d′) level and estimate a well depth at 298 K from their data of 31.9 kcal/mol. This is 3.4 kcal/mol different from Sheng et al.,[58] whose value is closer to data of Knyazev and Slagle,[59] 35.5 kcal/mol, Miller et al.,[60] 35.3 kcal/mol, and Blanksby et al.,[61] 35.7 kcal/mol.

The bond energies of $CH_3C(=O)OOH$ (Figure 2) and C_2H_5-OOH are compared in Table 6. The C−O, O−O, and O−H bond energies in $CH_3C(=O)OOH$ are 7−14 kcal/mol higher than those in C_2H_5OOH, probably because of coupling with the C=O bond in $CH_3C(=O)OOH$.

TABLE 6: Comparison of Bond Energies between $CH_3C(=O)OOH$ and C_2H_5OOH (Units: kcal/mol)

	$CH_3C(=O)OOH$	C_2H_5OOH
ROO−H	98.33	85.27
RO−OH	52.94	45.12
R−OOH	85.22	71.35
$H-CH_2C(=O)OOH$ or $H-CH_2CH_2OOH$	103.95	103.21

4.6. Analysis of Chemical Activation Reaction in Acetyl + O_2. QRRK calculations for $k(E)$ and master equation analysis for falloff are performed on this $CH_3C^{\bullet}O + O_2$ reaction system to estimate rate constants and to determine important reaction paths as a function of temperature and pressure (Tables 7 and 8).

The master equation analysis[42] uses an exponential-down model for the energy transfer function with $(\Delta E)^{\circ}_{down} = 1000$ cal/mol,[62,63] where N_2 is the third body (Table 7). Rate constants at 1atm pressure versus $1000/T$ are illustrated in Figure 3. Stabilization to ($CH_3C(=O)OO^{\bullet}$) is important below 600 K, with reverse dissociation important at higher temperatures. The diradical, $C^{\bullet}H_2CO(O^{\bullet})$, + OH product via RO−OH bond cleavage is also important above 1000 K, but it is 1 order of magnitude lower than reverse dissociation at 1000 K.

Plots of calculated rate constants for $CH_3C^{\bullet}O + O_2$ at 298 K versus pressure are illustrated in Figure 4. Stabilization is the dominant path above 0.01 atm, whereas reverse dissociation is important below 0.01 atm. $C^{\bullet}H_2CO(O^{\bullet})$ + OH is also important below 0.001 atm; but it is not important at atmospheric pressure, in agreement with Tyndall et al.[23]

Rate constants at 1000 K versus pressure are illustrated in Figure 5. Reverse dissociation is the dominant path at both high and low pressures. $C^{\bullet}H_2CO(O^{\bullet})$ + OH is more than 1 order of magnitude below reverse dissociation at 0.1 atm. Stabilization decreases as pressure is decreased (as expected).

We selected a high-pressure limit value of $k_1 = 2.65 \times 10^{12}$ cm^3/(mol s) for the acetyl radical + O_2 association as noted in Table 7 and described earlier. This results in a total forward rate constant of $(2.13 \pm 0.05) \times 10^{12}$ cm^3/(mol s) under the conditions of McDade et al.[20] and is about factor of 2 higher than their reported value of $(1.2 \pm 0.2) \times 10^{12}$ cm^3/(mol s) in 1−4 Torr He at 298 K.

4.7. Abstraction of Methyl Hydrogen in $CH_3C^{\bullet}O$ by O_2.

$$CH_3C^{\bullet}O + O_2 \rightarrow CH_2CO + HO_2 \qquad (12)$$

A transition state for direct abstraction of methyl hydrogens on $CH_3C^{\bullet}O$ by O_2 to form ketene plus HO_2 is identified with a barrier of 10 kcal/mol, at only the B3LYP/6-31G(d) level. This abstraction channel to form ketene + HO_2 is not competitive with the chemical activation $CH_3C^{\bullet}O$ by O_2 (association) rate constant to the same product set below 1400 K at 1 atm.

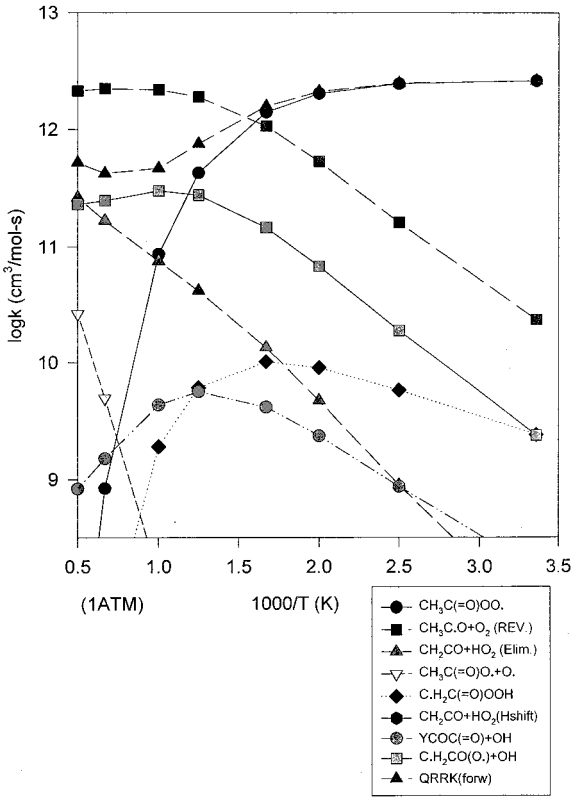

Figure 3. $CH_3C^{\bullet}O + O_2 \rightarrow$ products k vs $1000/T$ at 1 atm.

4.8. Unimolecular Dissociation of Acetyl Peroxy and Formyl Methyl Hydroperoxide Radicals. Stabilization of the adducts is observed to be important at lower temperature and moderate pressure conditions. Dissociation rate constants of the stabilized adducts are, therefore, of value. We estimated these dissociation rate parameters using QRRK analysis for $k(E)$ with master equation for falloff with a 0.5 kcal energy grain.

(1) $CH_3C(=O)OO^{\bullet}$ Dissociation. Plots of rate constants for $CH_3C(=O)OO^{\bullet}$ dissociation at 1 atm pressure versus $1000/T$ and rate constants at 298 and 1000 K versus pressure are illustrated in the Supporting Information (Figures 10S, 11S and 12S, respectively). H shift isomerization to $C^{\bullet}H_2C(=O)OOH$

TABLE 7: Input Parameters[a] and High-Pressure Limit Rate Constants (k_∞)[b] for QRRK Calculations[c]

Input Parameters for QRRK Calculations with Master Equation Analysis for Falloff
High-Pressure Limit Rate Constants

		k_∞	
reaction	A	n	E_a (kcal/mol)
1 $CH_3C^{\bullet}O + O_2 \rightleftharpoons CH_3C(=O)OO^{\bullet}$[d]	2.65×10^{12}	0.0	0.0
-1 $CH_3C(=O)OO^{\bullet} \rightleftharpoons CH_3C^{\bullet}O + O_2$[e]	3.37×10^{14}	0.0	32.44
2 $CH_3C(=O)OO^{\bullet} \rightleftharpoons C^{\bullet}H_2C(=O)OOH$[f]	1.29×10^{6}	2.00	24.57
3 $CH_3C(=O)OO^{\bullet} \rightleftharpoons CH_2CO + HO_2$[f]	9.47×10^{9}	1.17	34.45
4 $C^{\bullet}H_2C(=O)OOH \rightleftharpoons YCOC(=O) + OH$[f]	4.87×10^{13}	−0.29	20.77
5 $C^{\bullet}H_2C(=O)OOH \rightleftharpoons CH_2CO + HO_2$[f]	5.98×10^{11}	0.52	31.79
6 $C^{\bullet}H_2C(=O)OOH \rightleftharpoons C^{\bullet}H_2CO(O^{\bullet}) + OH$[f]	4.50×10^{15}[g]	0.00	24.59

[a] Geometric mean frequency (from CPFIT, ref 44: 361.7 cm^{-1}(6.059); 1143.8 cm^{-1} (8.297); 2566.9 cm^{-1} (2.645). Lennard-Jones parameters: $\sigma ij = 5.19$ Å, $\epsilon/k = 533.08$ K, ref 64. [b] The units of A factors and rate constants k are s^{-1} for unimolecular reactions and cm^3/(mol sec) for bimolecular reactions. [c] ΔE down of 1000 cal/mol is used, N_2 for bath gas. [Units] k_1: cm^3/(mol sec), $k_{-1} \rightarrow k_6$: s^{-1}. [d] $k_{\infty,1}$: Sehested et al.[24] [e] $k_{\infty,-1}$: Thermodynamics and microscopic reversibility. [f] A is calculated using TST and entropy of transition state, $\Delta S^{\ddagger}_{298}$ from HF/6-31G(d′) (see Table IVS.); E_a is from CBSQ calculation (see Table 4 and description for determination of E_a in Scheme 2). All parameters A, n, and E_a are fit over the temperature range of 298−2000 K. [g] Reference 65.

TABLE 8: Resulting Rate Constants in QRRK Calculations[a]

reaction	A	n	E_a (kcal/mol)	k_{298}
(1) Calculated Reaction Parameters at $P = 0.01$ atm, $k = A(T/K)^n \exp(-E_a/RT)$ ($298 \le T/K \le 2000$)				
1 $CH_3C^{\bullet}O + O_2 \rightleftharpoons CH_3C(=O)OO^{\bullet}$	9.04×10^{72}	−20.57	13.54	1.35×10^{12}
7 $CH_3C^{\bullet}O + O_2 \rightleftharpoons CH_2CO + HO_2$	2.21×10^{9}	0.72	2.82	1.15×10^{9}
8 $CH_3C^{\bullet}O + O_2 \rightleftharpoons YCOC(=O) + OH$	7.60×10^{24}	−4.76	3.42	3.97×10^{10}
9 $CH_3C^{\bullet}O + O_2 \rightleftharpoons C^{\bullet}H_2C(=O)OOH$	2.78×10^{69}	−19.51	14.89	1.79×10^{10}
10 $CH_3C^{\bullet}O + O_2 \rightleftharpoons C^{\bullet}H_2CO(O^{\bullet}) + OH$	7.79×10^{17}	−1.92	2.42	2.32×10^{11}
2 $CH_3C(=O)OO^{\bullet} \rightleftharpoons C^{\bullet}H_2C(=O)OOH$	3.03×10^{39}	−9.08	32.73	1.02×10^{-7}
3 $CH_3C(=O)OO^{\bullet} \rightleftharpoons CH_2CO + HO_2$	4.42×10^{56}	−15.38	42.76	1.69×10^{-13}
4 $C^{\bullet}H_2C(=O)OOH \rightleftharpoons YCOC(=O) + OH$	8.62×10^{10}	-0.36	16.62	7.17×10^{-3}
5 $C^{\bullet}H_2C(=O)OOH \rightleftharpoons CH_2CO + HO_2$	6.43×10^{-18}	6.33	19.96	6.79×10^{-17}
6 $C^{\bullet}H_2C(=O)OOH \rightleftharpoons C^{\bullet}H_2CO(O^{\bullet}) + OH$	2.03×10^{-5}	4.67	13.99	3.97×10^{-4}
(2) Calculated Reaction Parameters at $P = 0.1$ atm, $k = A(T/K)^n \exp(-E_a/RT)$ ($298 \le T/K \le 2000$)				
1 $CH_3C^{\bullet}O + O_2 \rightleftharpoons CH_3C(=O)OO^{\bullet}$	3.41×10^{69}	−18.90	14.40	1.62×10^{12}
7 $CH_3C^{\bullet}O + O_2 \rightleftharpoons CH_2CO + HO_2$	1.65×10^{12}	−0.10	4.60	3.93×10^{8}
8 $CH_3C^{\bullet}O + O_2 \rightleftharpoons YCOC(=O) + OH$	4.14×10^{27}	−5.49	6.17	3.20×10^{9}
9 $CH_3C^{\bullet}O + O_2 \rightleftharpoons C^{\bullet}H_2C(=O)OOH$	2.50×10^{64}	−17.49	15.49	5.81×10^{9}
10 $CH_3C^{\bullet}O + O_2 \rightleftharpoons C^{\bullet}H_2CO(O^{\bullet}) + OH$	1.47×10^{21}	−2.83	4.97	3.33×10^{10}
2 $CH_3C(=O)OO^{\bullet} \rightleftharpoons C^{\bullet}H_2C(=O)OOH$	1.17×10^{35}	−7.46	32.25	9.07×10^{-8}
3 $CH_3C(=O)OO^{\bullet} \rightleftharpoons CH_2CO + HO_2$	1.25×10^{54}	−13.84	44.10	3.22×10^{-13}
4 $C^{\bullet}H_2C(=O)OOH \rightleftharpoons YCOC(=O) + OH$	8.89×10^{15}	−1.86	18.15	1.09×10^{-2}
5 $C^{\bullet}H_2C(=O)OOH \rightleftharpoons CH_2CO + HO_2$	1.54×10^{-16}	6.15	18.35	8.81×10^{-15}
6 $C^{\bullet}H_2C(=O)OOH \rightleftharpoons C^{\bullet}H_2CO(O^{\bullet}) + OH$	5.44×10^{7}	0.99	17.22	3.61×10^{-3}
(3) Calculated Reaction Parameters at $P = 1$ atm, $k = A(T/K)^n \exp(-E_a/RT)$ ($298 \le T/K \le 2000$)				
1 $CH_3C^{\bullet}O + O_2 \rightleftharpoons CH_3C(=O)OO^{\bullet}$	5.79×10^{61}	−16.07	13.40	1.50×10^{12}
7 $CH_3C^{\bullet}O + O_2 \rightleftharpoons CH_2CO + HO_2$	2.04×10^{15}	−0.95	7.04	6.20×10^{7}
8 $CH_3C^{\bullet}O + O_2 \rightleftharpoons YCOC(=O) + OH$	3.24×10^{27}	−5.37	8.27	1.43×10^{8}
9 $CH_3C^{\bullet}O + O_2 \rightleftharpoons C^{\bullet}H_2C(=O)OOH$	7.40×10^{56}	−14.88	14.87	1.40×10^{9}
10 $CH_3C^{\bullet}O + O_2 \rightleftharpoons C^{\bullet}H_2CO(O^{\bullet}) + OH$	8.24×10^{22}	−3.26	7.48	2.31×10^{9}
2 $CH_3C(=O)OO^{\bullet} \rightleftharpoons C^{\bullet}H_2C(=O)OOH$	2.89×10^{29}	−5.55	31.11	8.15×10^{-8}
3 $CH_3C(=O)OO^{\bullet} \rightleftharpoons CH_2CO + HO_2$	1.38×10^{47}	−11.15	43.62	3.64×10^{-13}
4 $C^{\bullet}H_2C(=O)OOH \rightleftharpoons YCOC(=O) + OH$	6.24×10^{13}	−0.99	18.10	1.17×10^{-2}
5 $C^{\bullet}H_2C(=O)OOH \rightleftharpoons CH_2CO + HO_2$	2.30×10^{-24}	9.22	14.95	1.62×10^{-12}
6 $C^{\bullet}H_2C(=O)OOH \rightleftharpoons C^{\bullet}H_2CO(O^{\bullet}) + OH$	3.67×10^{8}	1.12	18.28	8.52×10^{-3}
(4) Calculated Reaction Parameters at $P = 10$ atm, $k = A(T/K)^n \exp(-E_a/RT)$ ($298 \le T/K \le 2000$)				
1 $CH_3C^{\bullet}O + O_2 \rightleftharpoons CH_3C(=O)OO^{\bullet}$	5.07×10^{52}	−12.96	11.56	1.46×10^{12}
7 $CH_3C^{\bullet}O + O_2 \rightleftharpoons CH_2CO + HO_2$	4.22×10^{15}	−0.97	8.82	5.71×10^{6}
8 $CH_3C^{\bullet}O + O_2 \rightleftharpoons YCOC(=O) + OH$	1.04×10^{25}	−4.53	9.89	3.57×10^{6}
9 $CH_3C^{\bullet}O + O_2 \rightleftharpoons C^{\bullet}H_2C(=O)OOH$	4.47×10^{49}	−12.44	14.33	2.29×10^{8}
10 $CH_3C^{\bullet}O + O_2 \rightleftharpoons C^{\bullet}H_2CO(O^{\bullet}) + OH$	1.99×10^{22}	−2.98	9.62	7.36×10^{7}
2 $CH_3C(=O)OO^{\bullet} \rightleftharpoons C^{\bullet}H_2C(=O)OOH$	4.44×10^{23}	−3.62	29.68	8.43×10^{-8}
3 $CH_3C(=O)OO^{\bullet} \rightleftharpoons CH_2CO + HO_2$	1.31×10^{39}	−8.32	42.28	3.33×10^{-13}
4 $C^{\bullet}H_2C(=O)OOH \rightleftharpoons YCOC(=O) + OH$	6.67×10^{8}	0.77	17.23	1.23×10^{-2}
5 $C^{\bullet}H_2C(=O)OOH \rightleftharpoons CH_2CO + HO_2$	1.95×10^{-21}	9.04	16.14	6.65×10^{-11}
6 $C^{\bullet}H_2C(=O)OOH \rightleftharpoons C^{\bullet}H_2CO(O^{\bullet}) + OH$	3.30×10^{5}	2.43	18.35	1.17×10^{-2}

[a] The units of A factors and rate constants k are s^{-1} for unimolecular reactions and $cm^3/(mol\ s)$ for bimolecular reactions.

is important below 500 K at 1atm pressure. Reverse dissociation and $C^{\bullet}H_2CO(O^{\bullet}) + OH$ are important above 1000 K.

(2) $C^{\bullet}H_2C(=O)OOH$ Dissociation. Rate constants for $C^{\bullet}H_2C(=O)OOH$ dissociation at 1 atm pressure versus $1000/T$ and rate constants at 298 and 1000 K versus pressure are illustrated in the Supporting Information (Figures 13S, 14S and 15S, respectively). At 1 atm, the diradical ($C^{\bullet}H_2CO(O^{\bullet})$) + OH product set is the dominant path above 800 K, with the $YCOC(=O) + OH$ also important below 400 K.

Products from the low-temperature reaction at both high and low pressure are $YCOC(=O) + OH$ products via OH elimination and H shift to the peroxy radical. The diradical ($C^{\bullet}H_2CO(O^{\bullet})$) + OH from RO−OH cleavage is also important above 1 atm at low temperature. At higher temperatures, the diradical ($C^{\bullet}H_2CO(O^{\bullet})$) + OH is the dominant path, as a result of the loose transition state structure. Products ratios from $C^{\bullet}H_2C(=O)OOH$ dissociation at 1 atm and 1000 K are listed in Table 9.

(3) Comparison of Dissociation Rate Constants between QRRK with Master Equation and ChemRate (RRKM with Master Equation). Dissociation rate constants at 800 and 1000 K versus pressure are compared between QRRK with master equation and ChemRate[66] (Rice−Ramsperger−Kassel−Marcus (RRKM) with master equation) on $CH_3C(=O)OO^{\bullet}$ dissociations in Figures 6 and 7 and for $C^{\bullet}H_2C(=O)OOH$ in Figures 8 and 9, respectively.

TABLE 9: Products Ratios from $C^{\bullet}H_2C(=O)OOH$ Dissociation at 1 atm and 1000 K

reactant	activated intermediate	product	ratio (%)
$C^{\bullet}H_2C(=O)OOH$	$\rightarrow C^{\bullet}H_2C(=O)OOH^*$	$\rightarrow YCOC(=O) + OH$	11.3
$C^{\bullet}H_2C(=O)OOH$	$\rightarrow C^{\bullet}H_2C(=O)OOH^*$	$\rightarrow C^{\bullet}H_2CO(O^{\bullet}) + OH$	86.3
$C^{\bullet}H_2C(=O)OOH$	$\rightarrow C^{\bullet}H_2C(=O)OOH^*$	$\rightarrow CH_2CO + HO_2$	0.0
$C^{\bullet}H_2C(=O)OOH$	$\rightarrow CH_3C(=O)OO^{\bullet *}$	$\rightarrow CH_3C^{\bullet}O + O_2$	0.04
$C^{\bullet}H_2C(=O)OOH$	$\rightarrow CH_3C(=O)OO^{\bullet *}$	$\rightarrow CH_2CO + HO_2$	0.0
$C^{\bullet}H_2C(=O)OOH$	$\rightarrow CH_3C(=O)OO^{\bullet *}$	$\rightarrow CH_3C(=O)OO^{\bullet}$	2.4

Calculated rate constants from the two methods versus pressure for $CH_3C(=O)OO^{\bullet}$ dissociation are compared in Figures 6 (800 K) and 7 (1000 K). The rate constants to $C^{\bullet}H_2C(=O)OOH$ (H shift isomerization) show very good agreement, with reasonable agreement also observed for predictions on dissociation to $CH_3C^{\bullet}O + O_2$. Chemrate predicts a slightly

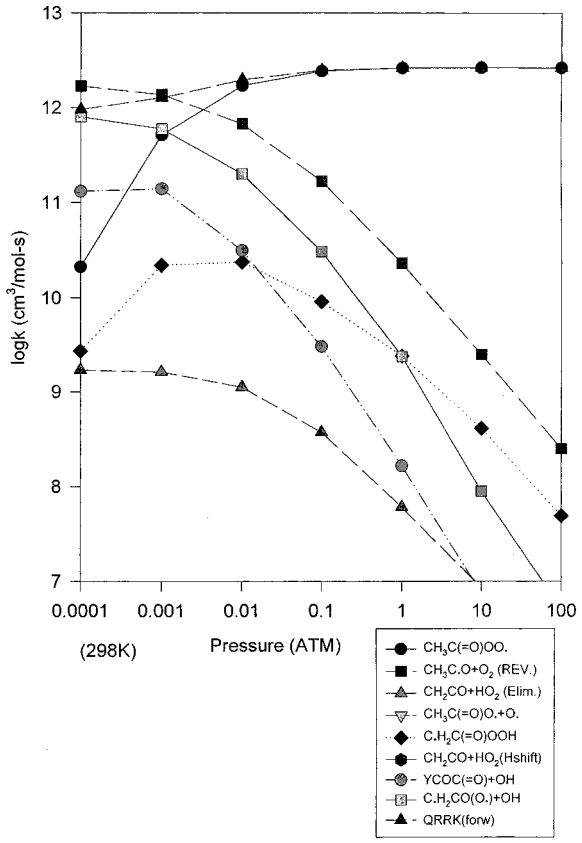

Figure 4. $CH_3C^{\bullet}O + O_2 \rightarrow$ products k vs pressure at 298 K.

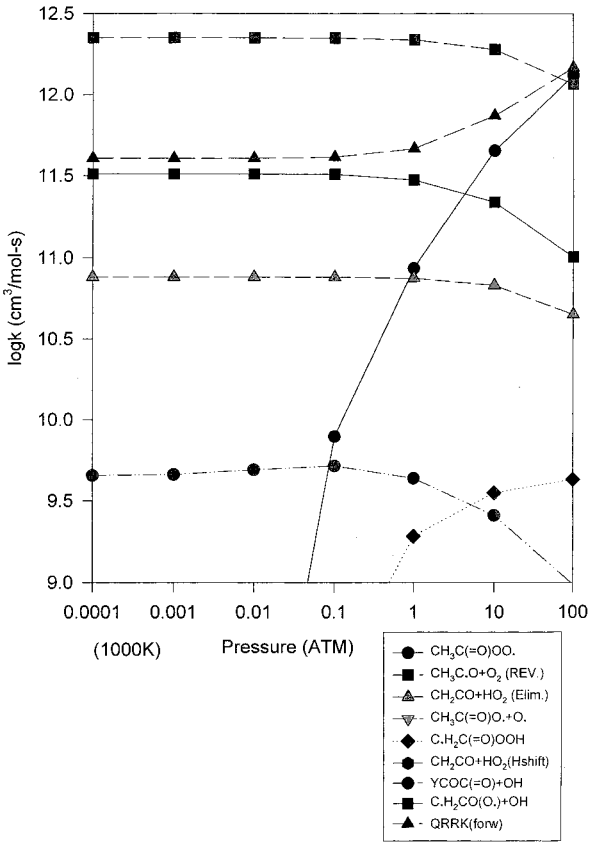

Figure 5. $CH_3C^{\bullet}O + O_2 \rightarrow$ products k vs pressure at 1000 K.

broader falloff for all of the three reaction paths, with the largest variation for the lowest rate channel of HO_2 elimination. This is amplified a bit in the 1000 K data of Figure 7.

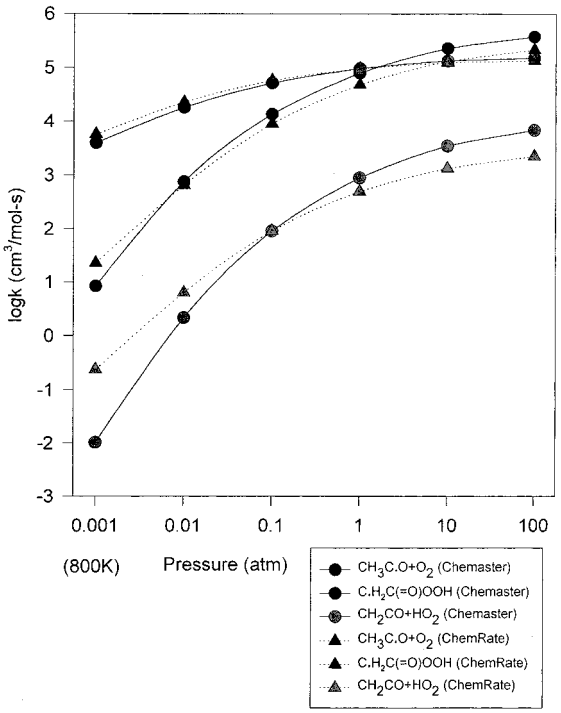

Figure 6. Comparison of rate constants between Chemaster and ChemRate with pressure in 800 K with $CH_3C(=O)OO^{\bullet}$ dissociation.

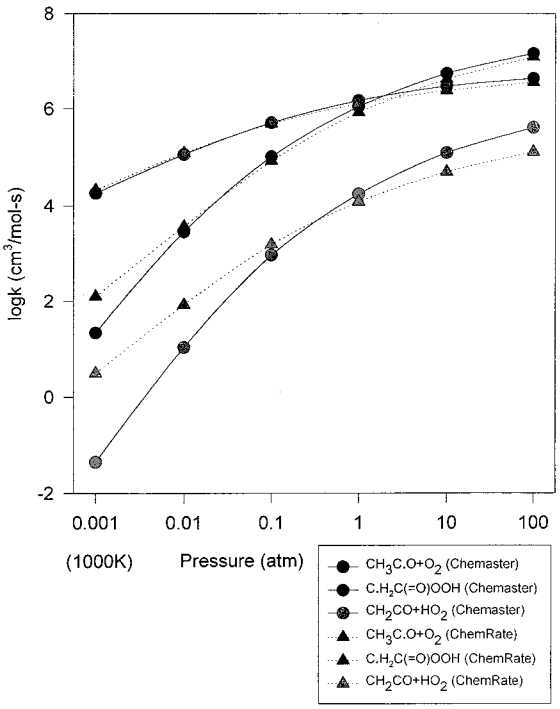

Figure 7. Comparison of rate constants between Chemaster and ChemRate with pressure in 1000 K with $CH_3C(=O)OO^{\bullet}$ dissociation.

$C^{\bullet}H_2C(=O)OOH$ dissociation rate constants versus pressure are compared in Figures 8 and 9 for 800 and 1000 K, respectively. The YCOC(=O) + OH products via OH elimination and H shift isomerization ($CH_3C(=O)OO^{\bullet}$) show agreement above 1 atm. The rate constants of ChemRate are 1.5−2 times higher than those calculated by use of QRRK with master equation below 0.1 atm in both figures.

4.9. Acetyl Radical Unimolecular Dissociation. The energy diagram for acetyl radical unimolecular dissociation is illustrated in Figure 10. The acetyl radical $CH_3C^{\bullet}O$ ($\Delta H^{\circ}_{f,298} = -3.08$ kcal/mol in CBSQ) can decompose to $CH_3 + CO$ ($E_a = 16.64$),

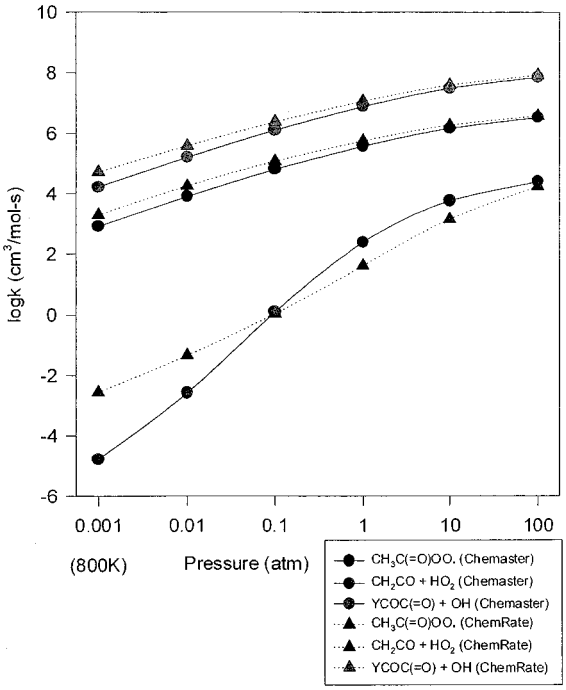

Figure 8. Comparison of rate constants between Chemaster and ChemRate with pressure in 800 K with $C^{\bullet}H_2C(=O)OOH$ dissociation.

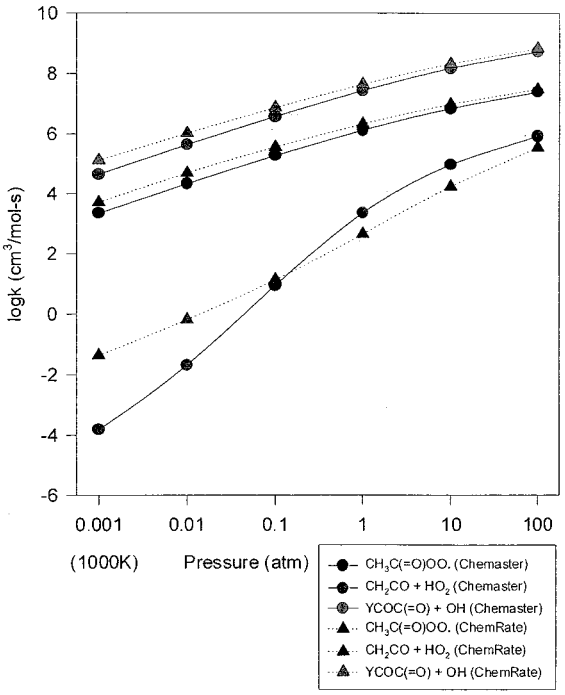

Figure 9. Comparison of rate constants between Chemaster and ChemRate with pressure in 1000 K with $C^{\bullet}H_2C(=O)OOH$ dissociation.

undergo β scission to products, $CH_2CO + H$ ($E_a = 43.17$), or isomerize via hydrogen shift ($E_a = 46.11$) to form the slightly higher energy $C^{\bullet}H_2CHO$ isomer ($\Delta H^{\circ}_{f,298} = 3.52$).

4.10. Detailed Mechanism of Acetyl Radical Reactions. A small detailed mechanism including the reactions evaluated in this study is assembled and listed in Table 10. The mechanism consists of 98 reactions and 37 species with each elementary reaction evaluated and referenced. The CHEMKIN II integrator computer code[67] is used to model the reaction conditions of Tyndall et al.[23] Abstraction reactions by O, H, OH, HO_2, O_2, and CH_3 radicals are taken from evaluated literature wherever possible. A procedure from Dean and Bozzelli[68] is used to estimate abstraction rate constants by H, HO_2, CH_3, and $CH_3C(=O)OO^{\bullet}$ radicals when no literature data are available. Abstraction reactions are not considered pressure dependent and therefore do not require falloff analysis.

The reactions of $CH_3CHO + OH \rightarrow CH_3C^{\bullet}O$ and $\rightarrow C^{\bullet}H_2CHO + H_2O$ are analyzed to model conditions of Tyndall et al., 0−0.01 s, 300 K, and 3 Torr, both with and without added O_2. The reaction with no O_2 added (mole fraction: $CH_3CHO = 1.2 \times 10^{-4}$, $OH = 3.6 \times 10^{-6}$) shows 99% $CH_3C^{\bullet}O$, acetyl radical, and 1% $C^{\bullet}H_2CHO$, formyl methyl radical, at 0.01 s via OH abstraction paths.

Data on concentration versus time for reaction conditions identical to those above, plus 3 Torr of O_2 (mole fraction $= 9.1 \times 10^{-4}$) are illustrated in Figure 11. $CH_3C(=O)OO^{\bullet}$, $C^{\bullet}H_2CO(O^{\bullet})$, and $YCOC(=O)$, which result from the acetyl radical reaction with O_2, are the major products. In the mechanism, the diradical, $C^{\bullet}H_2CO(O^{\bullet})$, dissociates to $^3CH_2 + CO_2$ which is 13 kcal/mol endothermic. Under these O_2 conditions, we observe that only 20% of the OH radical is regenerated through the acetyl radical with O_2 reaction. Tyndall et al.[23] and Michael et al.[27] both report almost complete regeneration of OH in their experiments.

Chemkin calculation of complete OH regeneration requires adjustment of the computed barrier from 26.42 down to 11.42 kcal/mol for reaction ($CH_3C(=O)OO^{\bullet} \rightarrow TCC(=O)OO^{\bullet}$) that forms OH. This adjustment of the barrier is probably unreasonable, and we continue to look for reactions that lead to regeneration of OH.

4.11. Importance of $CH_3C^{\bullet}O + O_2$ Relative to Unimolecular Dissociation of $CH_3C^{\bullet}O$. The competition between unimolecular dissociation of $CH_3C^{\bullet}O \rightarrow CH_3 + CO$ versus association of $CH_3C^{\bullet}O$ with O_2 as a function of reactor temperature is considered. We utilize the mechanism for this evaluation because the reaction system is complex; it involves reactions of chemical activated and stabilized $CH_3C(=O)OO^{\bullet}$. The $C^{\bullet}H_2C(=O)OOH$ isomer has low barriers for both forward and reverse reactions resulting in a quasiequilibria system. In addition, $CH_3C^{\bullet}O$ has a low energy dissociation path ($E_a = 16.64$ kcal/mol).

Several reaction condition sets are evaluated, one similar to those of Tyndall et al.[23] is 0.01 s with mole fraction of $CH_3CHO = 1.2 \times 10^{-4}$, $OH = 3.6 \times 10^{-6}$, and $O_2 = 9.1 \times 10^{-4}$. The reactions are evaluated at two pressures 1 Torr and 1 atm. The fraction of acetyl radical that reacts with O_2 versus unimolecular dissociation is summarized in Scheme 3. It shows that the two reaction channels, oxidation and dissociation, are competitive around 500 K. The unimolecular dissociation channel accounts for more than 80% of the reaction at 600 K.

The second condition set considers the competition between oxidation and dissociation at concentrations more relative to combustion. Mole fractions: ($CH_3C^{\bullet}O = 1.0 \times 10^{-5}$, $O_2 = 0.15$, $N_2 = 0.80$, and CH_4(fuel) $= 0.05$). Plots of concentration versus time for 10 ns, at 300 K, and 1 atm are illustrated in

Scheme 3: Fraction of Oxidation and Dissociation of Acetyl Radical ($t = 0.01$ s, mole fraction: $CH_3CHO = 1.2 \times 10^{-4}$, $OH = 3.6 \times 10^{-6}$, and $O_2 = 9.1 \times 10^{-4}$)

	oxidation		dissociation	
T/%	1 Torr	1 atm	1 Torr	1 atm
400K	93.3	99.8	6.7	0.2
450K	66.5	98.7	33.5	1.3
475K	46.3	96.6	53.7	3.4
500K	28.8	91.2	71.2	8.8
550K	9.7	43.1	90.3	56.9
600K	3.4	17.1	96.6	82.9

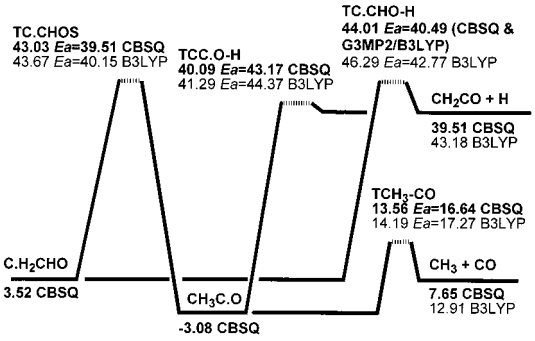

Figure 10. Potential energy diagram of acetyl and formyl methyl radical unimolecular isomerization/dissociations (units: kcal/mol).

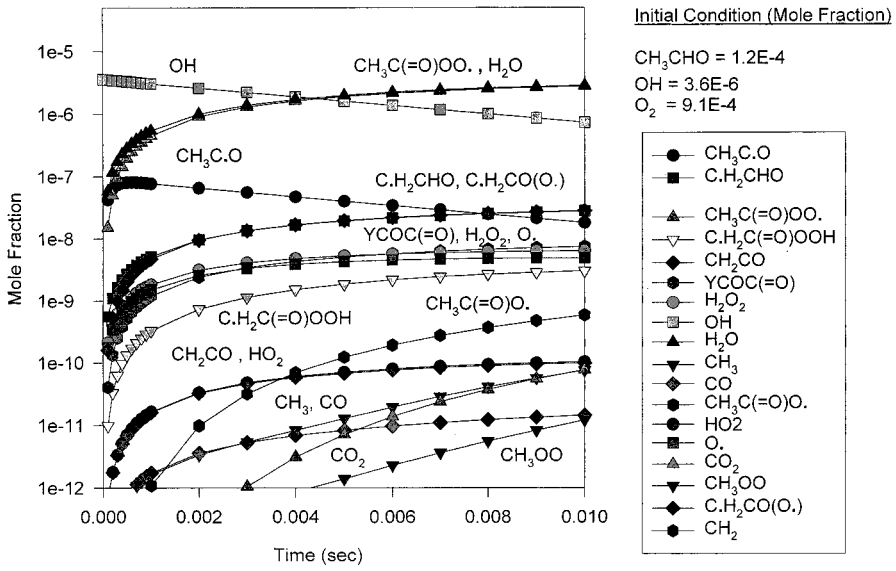

Figure 11. Chemkin kinetic calculations: concentration vs time.

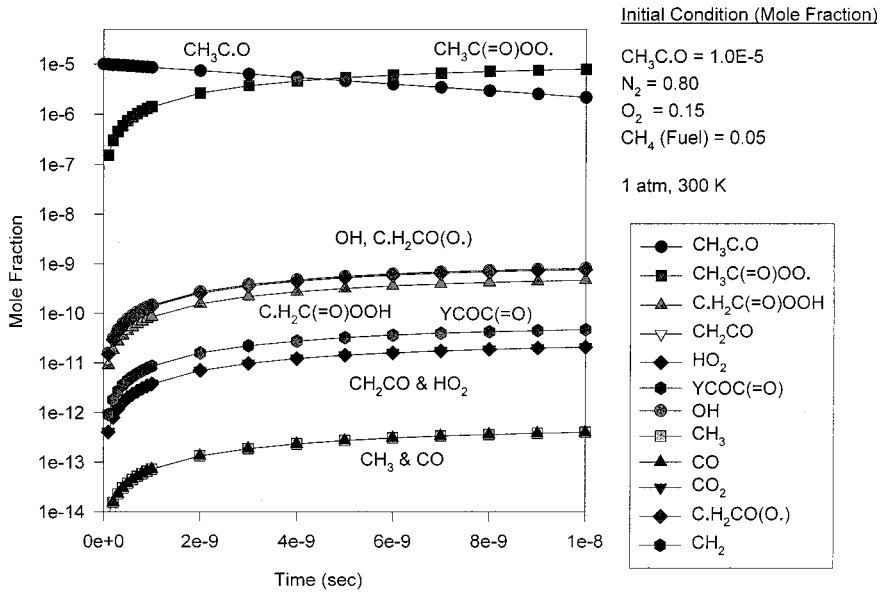

Figure 12. Chemkin kinetic calculations: concentration vs time.

Figure 12. The $CH_3C^{\bullet}O$ radicals decrease slowly with time, from the oxidation with effectively no unimolecular dissociation. At 0.1 s time, the ratio of oxidation to unimolecular dissociation products, $CH_3C(=O)OO^{\bullet}$: CO is 2.0×10^7:1. The $CH_3C^{\bullet}O$ radicals decrease by 3 orders magnitudes at 40 ns. The major product is stabilized $CH_3C(=O)OO^{\bullet}$ which results from acetyl radical reaction with O_2.

Products are illustrated in Figure 13 for reaction at higher temperature, 750 K, and 1 atm. The major products are $CH_3C(=O)OO^{\bullet}$, CH_3, and CO; these result from both acetyl radical reaction with O_2 and from $CH_3C^{\bullet}O$ unimolecular dissociation to $CH_3 + CO$. Above 800 K, the major products are CH_3 and CO from the unimolecular dissociation. The oxidation and dissociation channels are competitive around 750 K under these

TABLE 10: Detailed Mechaism

reactions		A	n	E_a	ref
CH_3CHO	$= CH_3+HCO$	6.99×10^{44}	−9.82	88320	*a*
CH_3CHO	$= CH_3C^{\bullet}O+H$	7.50×10^{44}	−11.49	92652	*a*
CH_3CHO+O_2	$= CH_3C^{\bullet}O+HO_2$	3.01×10^{13}	0.0	39143	*b*
HCO	$= H+CO$	7.94×10^{17}	−3.51	16326	*a*
$CH_3CHO+OH$	$= CH_3C^{\bullet}O+H_2O$	3.37×10^{12}	0.0	−536	*c*
CH_3CHO+O	$= CH_3C^{\bullet}O+OH$	1.08×10^{13}	0.0	2186	*c*
CH_3CHO+H	$= CH_3C^{\bullet}O+H_2$	4.00×10^{13}	0.0	4206	*d*
$CH_3CHO+HO_2$	$= CH_3C^{\bullet}O+H_2O_2$	3.01×10^{12}	0.0	8000	*b*
$CH_3CHO+CH_3$	$= CH_3C^{\bullet}O+CH_4$	1.86×10^{8}	0.0	2464	*b*
$CH_3CHO+OH$	$= C^{\bullet}H_2CHO+H_2O$	4.31×10^{11}	0.0	1000	*e*
CH_3CHO+H	$= C^{\bullet}H_2CHO+H_2$	2.4×10^{8}	1.5	2103	*f*
CH_3CHO+O	$= C^{\bullet}H_2CHO+OH$	5.85×10^{12}	0.0	1808	*b*
$CH_3CHO+HO_2$	$= C^{\bullet}H_2CHO+H_2O_2$	1.4×10^{4}	2.69	14068	*f*
$CH_3CHO+CH_3$	$= C^{\bullet}H_2CHO+CH_4$	8.1×10^{5}	1.87	5251	*f*
$CH_3C^{\bullet}O+O_2$	$= CH_3C(=O)OO^{\bullet}$	1.90×10^{76}	−22.20	12775	*a*
$CH_3C^{\bullet}O+O_2$	$= CH_2CO+HO_2$	3.29×10^{8}	0.96	2341	*a*
$CH_3C^{\bullet}O+O_2$	$= CH_3C(=O)O^{\bullet}+O^{\bullet}$	8.17×10^{13}	−0.33	21744	*a*
$CH_3C^{\bullet}O+O_2$	$= C^{\bullet}H_2C(=O)OOH$	3.91×10^{72}	−20.99	13932	*a*
$CH_3C^{\bullet}O+O_2$	$= CH_2CO+HO_2$	1.23×10^{6}	0.88	6367	*a*
$CH_3C^{\bullet}O+O_2$	$= YCOC(=O)+OH$	4.27×10^{21}	−3.84	1444	*a*
$CH_3C^{\bullet}O+O_2$	$= C^{\bullet}H_2CO(O^{\bullet})+OH$	1.11×10^{16}	−1.40	1250	*a*
$CH_3C(=O)OO^{\bullet}$	$= CH_3C^{\bullet}O+O_2$	1.65×10^{25}	−5.53	28017	*a*
$CH_3C(=O)OO^{\bullet}$	$= CH_2CO+HO_2$	8.37×10^{23}	−5.98	29810	*a*
$CH_3C(=O)OO^{\bullet}$	$= CH_3C(=O)O^{\bullet}+O^{\bullet}$	9.18×10^{7}	−6.66	46289	*a*
$CH_3C(=O)OO^{\bullet}$	$= C^{\bullet}H_2C(=O)OOH$	2.05×10^{17}	−2.30	24938	*a*
$C^{\bullet}H_2C(=O)OOH$	$= CH_2CO+HO_2$	4.06×10^{7}	−3.17	27150	*a*
$C^{\bullet}H_2C(=O)OOH$	$= YCOC(=O)+OH$	4.78×10^{20}	−3.73	19179	*a*
$C^{\bullet}H_2C(=O)OOH$	$= C^{\bullet}H_2CO(O^{\bullet})+OH$	1.18×10^{20}	−3.77	20459	*a*
$C^{\bullet}H_2C(=O)OOH$	$= CH_3C(=O)OO^{\bullet}$	8.33×10^{14}	−1.99	19173	*a*
$CH_3C(=O)O^{\bullet}$	$= CH_3+CO_2$	3.41×10^{15}	−0.48	17466	*a*
$C^{\bullet}H_2CO(O^{\bullet})$	$= CH_2+CO_2$	1.24×10^{11}	−0.85	16563	*a*
$C^{\bullet}H_2CHO+O_2$	$= CH_2(OO^{\bullet})CHO$	4.15×10^{64}	−18.13	15908	*a*
$C^{\bullet}H_2CHO+O_2$	$= CH_2CO+HO_2$	2.56×10^{5}	2.57	23785	*a*
$C^{\bullet}H_2CHO+O_2$	$= CH_2(OOH)C^{\bullet}(=O)$	2.67×10^{50}	−18.89	15625	*a*
$C^{\bullet}H_2CHO+O_2$	$= CH_2CO+HO_2$	2.88×10^{-3}	2.06	4400	*a*
$C^{\bullet}H_2CHO+O_2$	$= CO+CH_2O+OH$	5.77×10^{14}	−0.96	5752	*a*
$CH_2(OO^{\bullet})CHO$	$= C^{\bullet}H_2CHO+O_2$	2.75×10^{51}	−13.62	33711	*a*
$CH_2(OO^{\bullet})CHO$	$= CH_2CO+HO_2$	1.81×10^{29}	−12.65	46998	*a*
$CH_2(OO^{\bullet})CHO$	$= CH_2(OOH)C^{\bullet}(=O)$	5.31×10^{34}	−8.00	26153	*a*
$CH_2(OOH)C^{\bullet}(=O)$	$= CH_2CO+HO_2$	3.02×10^{3}	−4.73	21783	*a*
$CH_2(OOH)C^{\bullet}(=O)$	$= CO+CH_2O+OH$	3.93×10^{18}	−3.43	8668	*a*
$CH_2(OOH)C^{\bullet}(=O)$	$= CH_2(OO^{\bullet})CHO$	2.14×10^{6}	−4.59	16759	*a*
$CH_3C^{\bullet}O$	$= CH_2CO+H$	2.33×10^{-23}	1.64	38980	*a*
$CH_3C^{\bullet}O$	$= CH_3+CO$	4.87×10^{6}	0.33	12525	*a*
$CH_3C^{\bullet}O$	$= C^{\bullet}H_2CHO$	7.10×10^{-25}	1.48	39974	*a*
$C^{\bullet}H_2CHO$	$= CH_2CO+H$	1.43×10^{38}	−8.75	46719	*a*
$C^{\bullet}H_2CHO$	$= CH_3C^{\bullet}O$	5.84×10^{38}	−9.08	46719	*a*
$2CH_3C(=O)OO^{\bullet}$	$= 2CH_3C(=O)O^{\bullet}+O_2$	8.51×10^{10}	0.0	248	*g*
$CH_3CHO+CH_3C(=O)OO^{\bullet}$	$=CH_3C(=O)OOH+CH_3C^{\bullet}O$	2.4×10^{8}	1.5	3643	*f*
$CH_3CHO+CH_3C(=O)OO^{\bullet}$	$=CH_3C(=O)OOH+C^{\bullet}H_2CHO$	2.4×10^{8}	1.5	7933	*f*
$CH_2(OO^{\bullet})CHO+NO$	$= CH_2(O^{\bullet})CHO+NO_2$	1.26×10^{12}	0.0	1133	*h*
$CH_2(O^{\bullet})CHO$	$= CH_2O+HCO$	8.72×10^{22}	−4.9	12378	*a*
$CH_2(O^{\bullet})CHO$	$= CHOCHO+H$	2.94×10^{13}	−2.2	28503	*a*
$CH_3C(=O)OO^{\bullet}+NO$	$= CH_3C(=O)O^{\bullet}+NO_2$	1.26×10^{12}	0.0	1133	*h*
$C^{\bullet}H_2C(=O)OOH+O_2$	$= (^{\bullet}OO)\,H_2CC(=O)OOH$	1.10×10^{11}	0.0	0	*i*
$(^{\bullet}OO)H_2CC(=O)OOH+NO$	$=(^{\bullet}O)H_2CC(=O)OOH+NO_2$	1.26×10^{12}	0.0	1133	*h*
$(^{\bullet}O)H_2CC(=O)OOH$	$= C^{\bullet}H(=O)OOH+CH_2O$	1.35×10^{12}	0.0	20800	*a*
$C^{\bullet}H(=O)OOH$	$= CO+HO_2$	1.73×10^{10}	0.0	16550	*a*
$C^{\bullet}H(=O)OOH$	$= CO_2+OH$	3.34×10^{12}	0.0	24290	*a*
CH_3+O_2	$= CH_2O+OH$	2.61×10^{8}	1.01	12487	*j*
CH_3+O_2	$= CH_3OO$	1.99×10^{31}	−6.72	4212	*j*
CH_3OO	$= CH_2O+OH$	1.99×10^{20}	−7.76	47315	*a*
CH_3+CH_2O	$= HCO+CH_4$	5.54×10^{3}	2.81	5862	*k*
CH_3+HO_2	$= CH_3O+OH$	1.81×10^{13}	0.0	0	*b*
CH_3O	$= CH_2O+H$	6.13×10^{28}	−5.65	31351	*j*
CH_3O+HO_2	$= CH_2O+H_2O_2$	3.01×10^{11}	0.0	0	*k*
CH_2O+O	$= OH+HCO$	1.81×10^{13}	0.0	3080	*k*
CH_2O+H	$= H_2+HCO$	2.29×10^{10}	1.05	3279	*b*
CH_2O+OH	$= H_2O+HCO$	3.44×10^{9}	1.18	−447	*b*
$HCO+O_2$	$= CO+HO_2$	6.25×10^{15}	−1.15	2018	*j*
$HCO+O_2$	$= CO_2+OH$	5.45×10^{14}	−1.15	2018	*j*
$CO+O$	$= CO_2$	6.17×10^{14}	0.0	3001	*k*
$CO+OH$	$= CO_2+H$	6.32×10^{6}	1.5	−497	*k*
$CO+HO_2$	$= CO_2+OH$	1.51×10^{14}	0.0	23650	*k*

TABLE 10 (Continued)

reactions		*A*	*n*	E_a	ref
$CO+O_2$	$=CO_2+O$	2.53×10^{12}	0.0	47693	*k*
$H+O_2+M$	$=HO_2+M$	1.41×10^{18}	−0.8	0	*b*
$H+O_2$	$=OH+O$	1.99×10^{14}	0.0	16802	*b*
$OH+OH$	$=O+H_2O$	1.51×10^{9}	1.14	99	*b*
H_2+OH	$=H_2O+H$	1.02×10^{8}	1.6	3300	*b*
$H+OH+M$	$=H_2O+M$	2.21×10^{22}	−2.0	0	*b*
$O+HO_2$	$=OH+O_2$	1.75×10^{13}	0.0	−397	*l*
$OH+HO_2$	$=H_2O+O_2$	1.45×10^{16}	−1.0	0	*k*
$H+HO_2$	$=OH+OH$	1.69×10^{14}	0.0	874	*k*
$H+HO_2$	$=H_2+O_2$	6.62×10^{13}	0.0	2126	*k*
$H+HO_2$	$=H_2O+O$	3.01×10^{13}	0.0	1721	*b*
$H+O+M$	$=OH+M$	4.71×10^{18}	−1.0	0	*k*
H_2O_2+M	$=OH+OH+M$	1.21×10^{17}	0.0	45507	*b*
H_2O_2+OH	$=H_2O+HO_2$	1.75×10^{12}	0.0	318	*l*
H_2O_2+O	$=OH+HO_2$	9.63×10^{6}	2.0	3974	*k*
H_2O_2+H	$=OH+H_2O$	2.41×10^{13}	0.0	3974	*k*
H_2O_2+H	$=HO_2+H_2$	4.82×10^{13}	0.0	7949	*k*
CH_4+HO_2	$=H_2O_2+CH_3$	9.04×10^{12}	0.0	24641	*b*
$2HO_2$	$=2OH+O_2$	1.00×10^{12}	0.0	11500	*j*
HO_2+HO_2	$=H_2O_2+O_2$	1.87×10^{12}	0.0	1540	*b*
$H+H+M$	$=H_2+M$	5.44×10^{18}	−1.3	0	*k*
$O+H_2$	$=OH+H$	5.12×10^{4}	2.67	6285	*b*

[a] From QRRK calculations (1 Torr, 298−2000K). [b] Reference 69. [c] Reference 70. [d] Reference 71. [e] Reference 72. [f] Estimate in this study. [g] $2C_2H_5OO^{\bullet} = 2C_2H_5O^{\bullet} + O_2$ (ref 58). [h] Reference 73. [i] $0.7 \times 1.57 \times 10^{11}(C^{\bullet}H_2CHO + O_2)$. [j] Reference 65. [k] Reference 74. [l] Reference 75.

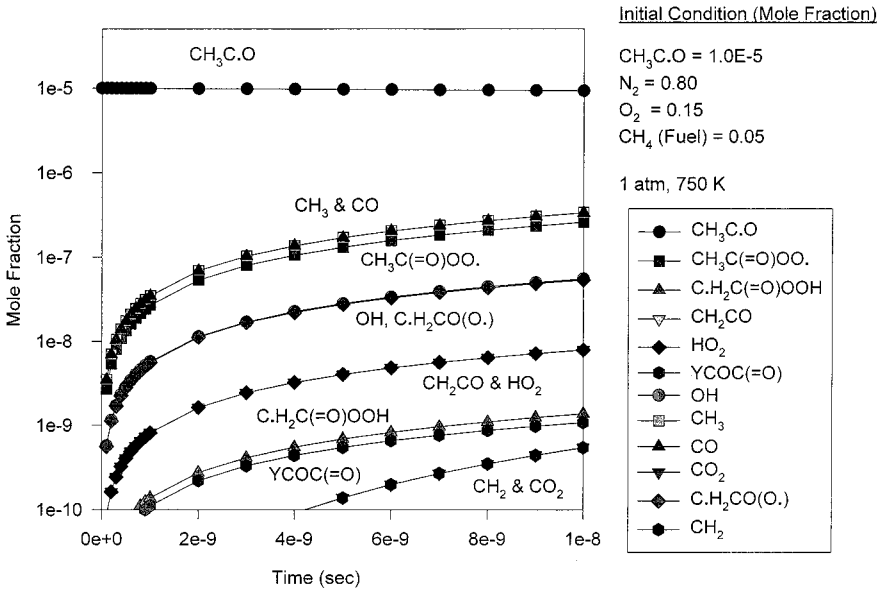

Figure 13. Chemkin kinetic calculations: concentration vs time.

Scheme 4: Fraction of Oxidation and Dissociation of Acetyl Radical (t = 10 ns, mole fraction: $CH_3C^{\bullet}O = 1.0 \times 10^{-5}$, $O_2 = 0.15$, $N_2 = 0.80$, and CH_4(fuel) = 0.05)

T/%	oxidation	dissociation	disso./oxi.
300K	100.0	0.0	0.00
500K	99.9	0.1	0.00
600K	97.8	2.2	0.02
700K	73.0	27.0	0.37
750K	43.6	56.4	1.29
800K	19.4	80.6	4.16
900K	2.8	97.2	34.93
1000K	0.4	99.6	232.51

conditions. Ratios of the product sets are summarized in Scheme 4 at varied temperature. These data are in reasonable agreement with the relative rate constant at these conditions. (Table VS and VIS)

5. Summary

Thermochemical properties of stable radicals and transition states on the $CH_3C^{\bullet}O + O_2$ reaction system are calculated using density functional and ab initio methods with enthalpies of formation ($\Delta H^{\circ}_{f,298}$) at the CBSQ level. Entropies (S°_{298}) and heat capacities ($C_p(T)$) are also determined, with inclusion of internal rotor contributions. The acetyl + O_2 system has a similar well depth to that of the more studied ethyl + O_2 system, but subsequent reaction barriers are significantly different. Reaction paths and kinetics are analyzed on $CH_3C^{\bullet}O + O_2$ reaction system using QRRK for $k(E)$ and master equation for falloff. Reaction to products is evaluated versus both pressure and temperature.

The major reaction path at 1atm pressure is the stabilization of peroxy adduct ($CH_3C(=O)OO^{\bullet}$) below 600 K. Reverse dissociation exhibits the highest rate constant for both the energized and stabilized adduct above 800 K. The major product channels are the diradical, ($C^{\bullet}H_2C(=O)O^{\bullet}$), + OH and ketene + HO_2 paths above 1000 K at 1 atm. It is important to further analyze the reaction products that result from this diradical.

A detailed reaction mechanism is constructed with pressure dependence for the acetyl radical reaction with O_2. Several paths

lead to formation (regeneration) of the OH radical as reported in experimental studies, but use of the mechanism for evaluation of the OH regeneration shows results that are low compared to experiment. The mechanism is also used to compare the competition between acetyl radical decomposition and acetyl radical reaction with O_2 with temperature.

Acknowledgment. We acknowledge the USEPA Northeast Regional Research Center and the USEPA Airborne Organics Research Center for funding. We would also like to thank to C. Sheng for the SMCPS program.

Nomenclature

C = carbon with hydrocarbons
assumed to satisfy respective valance
T = Transition state
• = radical site
= = double bond
− = bond [leaving/formed]
Y = Cyclic

Supporting Information Available: Optimized geometries at the MP2/6-31G(d′) and B3LYP/6-31G(d) levels for intermediate radicals and transition states (Figures 1S−9S). Plots of rate constants at 1 atm pressure versus 1000/*T*, and at 298 and 1000 K versus pressure for acetyl peroxy and formyl methyl hydroperoxy radical dissociation (Figures 10S−15S). Tables of total energies, zero-point vibrational energies, and thermal corrections for CBSQ calculation and vibrational frequencies and moments of inertia at the HF/6-31G(d′) level of calculation (Tables IS−IIIS). Tables of thermochemical analysis for reactions and ratio of rate constants and ratio of high-pressure limit rate constants between unimolecular dissociation of $CH_3C^{\bullet}O$ versus association of $CH_3C^{\bullet}O$ with O_2 (Tables IVS−VIS). This material is available free of charge via the Internet at http://pubs.acs.org.

References and Notes

(1) Benson, S. W. *Thermochemical Kinetics*; John Wiley and Sons: New York, 1976.
(2) Slagle, I. R.; Ratajaczak, E.; Gutman, D. J. *J. Phys. Chem.* **1986**, *90*, 402.
(3) Lightfoot, P. D.; Cox, R. A.; Crowley, J. N.; Destriau, M.; Hayman, G. D.; Jenkin, M. E.; Moortgat, G. K.; Zabel, F. *Atmos. Environ.* **1992**, *26A*, 1805.
(4) Atkinson, R. *Atmos. Environ.* **1990**, *24*A, 1.
(5) Slagle, I. R.; Feng, Q.; Gutman, D. *J. Phys. Chem.* **1984**, *88*, 3648.
(6) Clifford, E. P.; Farrell, J. T.; DeSain, J. D.; Taatjes, C. A. *J. Phys. Chem. A* **2000**, *104*, 11549.
(7) Tyndall, G. S.; Orlando, J. J.; Wallington, T. J.; Hurley, M. D. *Int. J. Chem. Kinet.* **1997**, *29*, 655.
(8) McAdam, G. K.; Walker, R. W. *J. Chem. Soc., Faraday Trans.* 2 **1987**, *83*, 1509.
(9) Plumb, I. C.; Ryan, K. R. *Int. J. Chem. Kinet.* **1981**, *13*, 1011.
(10) Kaiser, E. W.; Rimai, L.; Wallington, T. J. *J. Phys. Chem.* **1989**, *93*, 4094.
(11) Kaiser, E. W.; Rimai, L.; Wallington, T. J. *J. Phys. Chem.* **1990**, *94*, 3394.
(12) Gutman, D. *J. Chem. Phys.* **1987**, *84*, 409.
(13) Gulati, S. K.; Walker, R. W. *J. Chem. Soc., Faraday Trans.* 2 **1988**, *84*, 401.
(14) Rienstra-Kiracofe, J. C.; Allen, W. D.; Schaefer, H. F., III. *J. Phys. Chem. A* **2000**, *104*, 9840.
(15) Bozzelli, J. W.; Dean, A. M. *J. Phys. Chem.* **1990**, *94*, 3313.
(16) Wagner, A. F.; Slagle, I. R.; Sarzynski, D.; Gutman, D. *J. Phys. Chem.* **1990**, *94*, 1853.
(17) Baldwin, R. W.; Dean, C. E.; Walker, R. W. *J. Chem. Soc., Faraday Trans. 2* **1986**, *82*, 1445.
(18) Chen, C. J.; Bozzelli, J. W. *J. Phys. Chem. A* **2000**, *104*, 4997.
(19) McMillan, G. R.; Calvert, J. G. *Oxid. Combust. Rev.* **1965**, 83.
(20) McDade, C. E.; Lenhardt, T. M.; Bayes, K. D. *J. Photochem.* **1982**, *20*, 1.
(21) Atkinson, R.; Baulch, D. L.; Cox, R. A.; Hampson, R. F.; Kerr, J. A.; Rossi, M. J.; Troe, J. *J. Chem. Phys. Ref. Data* **1997**, *26*, 521.
(22) Maricq, M. M.; Szente, J. J. *J. Chem. Phys. Lett.* **1996**, *253*, 333.
(23) Tyndall, G. S.; Staffelbach, T. A.; Orlando, J. J.; Calvert, J. G. *Int. J. Chem. Kinet.* **1995**, *27*, 1009.
(24) Sehested, I.; Christensen, L. K.; Nielsen, O. J.; Wallington, T. J. *Int. J. Chem. Kinet.* **1998**, *30*, 913.
(25) Atkinson, R.; Baulch, D. L.; Cox, R. A.; Hampson, R. F., Jr.; Kerr, J. A.; Troe, J. *J. Phys. Chem. Ref. Data* **1989**, *18*, 881.
(26) Bartels, M.; Hoyermann, K. *An. Asoc. Quim. Argent.* **1985**, *73*, 253.
(27) Michael, J. V.; Keil, D. G.; Klemm, R. B. *J. Chem. Phys.* **1985**, *83*, 1630.
(28) Slagle, I. R.; Gutman, D. *J. Am. Chem. Soc.* **1982**, *104*, 4741.
(29) Alvarez-Idaboy, J. R.; Mora-Diez, N.; Boyd, R. J.; Vivier-Bunge, A. *J. Am. Chem. Soc.* **2001**, *123*, 2018.
(30) Aloisio, S.; Francisco, J. S. *J. Phys. Chem. A* **2000**, *104*, 3211.
(31) Zhu, L.; Johnston, G. *J. Phys. Chem.* **1995**, *99*, 15114.
(32) Stewart, J. J. P., *MOPAC 6.0*, Frank J. Seiler Research Lab., US Air Force Academy: Colorado, 1990.
(33) Frisch, M. J.; Trucks, G. W.; Schlegel, H. B.; Gill, P. M. W.; Johnson, B. G.; Robb, M. A.; Cheeseman, J. R.; Keith, T.; Petersson, G. A.; Montgomery, J. A.; Raghavachari, K.; Al-Laham, M. A.; Zakrzewski, V. G.; Ortiz, J. V.; Foresman, J. B.; Cioslowski, J.; Stefanov, B. B.; Nanayakkara, A.; Challacombe, M.; Peng, C. Y.; Ayala, P. Y.; Chen, W.; Wong, M. W.; Andres, J. L.; Replogle, E. S.; Gomperts, R.; Martin, R. L.; Fox, D. J.; Binkley, J. S.; Defrees, D. J.; Baker, J.; Stewart, J. P.; Head-Gordon, M.; Gonzalez, C.; Pople, J. A. *Gaussian 94*, revision C.2; Gaussian, Inc.: Pittsburgh, PA, 1995.
(34) Petersson, G. A.; Bennett, A.; Tensfeldt, T. G.; Al-Laham, M. A.; Shirley, W. A.; Mantzaris, J. *J. Chem. Phys.* **1988**, *89*, 2193.
(35) Petersson, G. A.; Tensfeldt, T. G.; Montgomery, J. A., Jr. *J. Chem. Phys.* **1991**, *94*, 6091.
(36) Ochterski, J. W.; Petersson, G. A.; Montgomery, J. A., Jr. *J. Chem. Phys.* **1996**, *104*, 2598.
(37) Nyden, M. R.; Petersson, G. A. *J. Chem. Phys.* **1991**, *75*, 1843.
(38) Petersson, G. A. *J. Chem. Phys.* **1994**, *94*, 6081.
(39) Montgomery, J. A., Jr.; Petersson, G. A. *J. Phys. Chem.* **1994**, *101*, 5900.
(40) Hehre, W. J.; Radom, L.; Schleyer, P. R.; Pople, J. A. *Ab Initio Molecular Orbital Theory*; John Wiley & Sons: New York, 1986.
(41) Pitzer, K. S.; Gwinn, W. D. *J. Chem. Phys.* **1942**, *10*, 428.
(42) Sheng, C.; Bozzelli, J. W.; Dean, A. M.; Chang, A. Y. *J. Phys. Chem. A* submitted.
(43) Chang, A. Y.; Bozzelli, J. W.; Dean, A. M. *Int. J. Res. Phys. Chem. Chem. Phys. (Z. Phys. Chem.)* **2000**, *214*, 1533.
(44) Bozzelli, J. W.; Chang, A. Y.; Dean, A. M. *Int. J. Chem. Kinet.* **1997**, *29*, 161.
(45) Petersson, G.; Schwartz, M. Personal communication.
(46) Eckart, C. *Phys. Rev.* **1930**, *35*, 1203.
(47) Schwartz, M.; Marshall, P.; Berry, R. J.; Ehlers, C. J.; Petersson, G. A. *J. Phys. Chem. A* **1998**, *102*, 10074
(48) Rodgers, A. S. *Selected Values for Properties of Chemical Compounds*; Thermodynamic Research Center, Texas A&M University: College Station, TX, 1982.
(49) Pedley, J. B.; Naylor, R. O.; Kirby, S. P. *Thermodynamic Data of Organic Compounds*, 2nd ed.; Chapman and Hall: London, 1986.
(50) Stull, D. R.; Prophet, H. *JANAF Thermochemical Tables*, 2nd ed. (NSRDS− NBS37); U.S. Government Printing Office: Washington DC, 1970.
(51) Stull, D. R.; Westrum, E. F., Jr.; Sinke, G. C. *The Chemical Thermodynamics of Organic Compounds*; Robert E. Krieger Publishing: Malabar, FL, 1987.
(52) Marshall, P. *J. Phys. Chem. A* **1999**, *103*, 4560.
(53) Mayer, P. M.; Glukhovtsev, M. N.; Gauld, J. W.; Radom, L. *J. Am. Chem. Soc.* **1997**, *119*, 12889.
(54) Zhu, L.; Bozzelli, J. W. *J. Phys. Chem. A* **2002**, *106*, 345.
(55) Lay, T. H.; Bozzelli, J. W. *J. Phys. Chem.* **1997**, *101*, 9505.
(56) Ritter, E. R.; Bozzelli, J. W. *Int. J. Chem. Kinet.* **1991**, *23*, 767.
(57) Ritter, E. R. *J. Chem. Info. Comput. Sci.* **1991**, *31*, 400.
(58) Sheng, C.; Bozzelli, J. W.; Dean, A. M. *2nd Joint Meeting of the U.S. Section*; The Combustion Institute: Oakland, CA, 2001.

(59) Knyazev, V. D.; Slagle, I. R. *J. Phys. Chem. A* **1998**, *102*, 1770.
(60) Miller, J. A.; Klippenstein, S. J.; Robertson, S. H. *28th Symposium (Int.) on Combustion*; The Combustion Institute: Edinburgh, U.K., 2000; p 1479.
(61) Blanksby, S. J.; Ramond, T. M.; Davico, G. E.; Nimlos, M. R.; Kato, S.; Bierbaum, V. M.; Carl Lineberger, W.; Ellison, G. B.; Okumura, M. *J. Am. Chem. Soc.* **2001**, *123*, 9585.
(62) Troe, J. In *Combustion Chemistry;* Gardiner, W. C., Jr., Ed.; Springer-Verlag: New York, 1984.
(63) Knyazev, V. D. *J. Phys. Chem.* **1996**, *100*, 5318.
(64) Reid, R. C.; Prausnitz, J. M.; Sherwood, T. K. *The Properties of Gases and Liquids*; McGraw-Hill Co.: New York, 1979.
(65) Chen, C.; Bozzelli, J. W. *J. Phys. Chem. A* **1999**, *103*, 9731.
(66) Mokrushin, V.; Bedanov, V.; Tsang, W.; Zachariah, M.; Knyazev, V. *ChemRate Computer Program*, version 1.10; NIST: Gaithersburg, MD, 1999.
(67) Kee, R. J.; Rupley, F. M.; Miller, J. A. *Chemkin-II: A Fortran Chemical Kinetics Package for the Analysis of Gas-Phase Chemical Kinetics*; Sandia National Laboratories: CA, 1989.
(68) Dean, A. M.; Bozzelli, J. W. In *Gas-Phase Combustion Chemistry, Chapter 2: Combustion Chemistry of Nitrogen*; Gardiner, W. C., Jr., Ed.; Springer-Verlag: New York, 1999.
(69) Baulch, D. L.; Cobos, C. J.; Cox, R. A.; Esser, C.; Frank, P.; Just, Th.; Kerr, J. A.; Pilling, M. J.; Troe, J.; Walker, R. W.; Warnatz, J. *J. Phys. Chem. Ref. Data* **1992**, *21*, 411.
(70) DeMore, W. B.; Sander, S. P.; Golden, D. M.; Hampson, R. F.; Kurylo, M. J.; Howard, C. J.; Ravishankara, A. R.; Kolb, C. E.; Molina, M. J. *JPL Pub.* **1997**, *4*, 1.
(71) Warnatz, J. In *Combustion Chemistry*, Gardiner, W. C., Jr., Ed.; Springer-Verlag: New York, 1984.
(72) Taylor, P. H.; Rahman, M. S.; Arif, M.; Dellinger, B.; Marshall, P. *26th Symposium (Int.) on Combustion*; The Combustion Institute: Pittsburgh, PA, 1996; p 497.
(73) Maricq, M. M.; Szente, J. J. *J. Phys. Chem.* **1996**, *100*, 12380.
(74) Tsang, W.; Hampson, R. F. *J. Phys. Chem. Ref. Data* **1986**, *15*, 1087.
(75) Ernst, J.; Spindler, K.; Wagner, H. Gg. *Ber. Bunsen-Ges. Phys. Chem.* **1976**, *80*, 645.